Effect of iron and sulfur on the solubility of highly siderophile elements in silicate melts

Dissertation

zur

Erlangung des Doktorgrades (Dr. rer. nat.)

der

Mathematisch-Naturwissenschaftlichen Fakultät

der

Rheinischen Friedrich-Wilhelms-Universität Bonn

vorgelegt von

Vera Laurenz

aus Steinfurt

Bonn,

Februar 2012

Angefertigt mit Genehmigung der Mathematisch-Naturwissenschaftlichen Fakultät der
Rheinischen Friedrich-Wilhelms-Universität Bonn

1. Gutachter: Prof. Dr. Christian Ballhaus
2. Gutachter: Prof. Dr. Thorsten Geisler-Wierwille
Tag der Promotion: 04. Mai 2012
Erscheinungsjahr 2012

An Eides statt versichere ich, dass

die vorgelegte Arbeit – abgesehen von den ausdrücklich bezeichneten Hilfsmitteln – persönlich, selbständig und ohne Benutzung anderer als der angegebenen Hilfsmittel angefertigt wurde,

die aus anderen Quellen direkt oder indirekt übernommenen Daten und Konzepte unter Angabe der Quelle kenntlich gemacht sind,

die vorgelegte Arbeit oder ähnliche Arbeiten nicht bereits anderweitig als Dissertation eingereicht worden ist bzw. sind,

für die inhaltlich-materielle Erstellung der vorgelegten Arbeit keine fremde Hilfe, insbersondere keine entgeltlich Hilfe von Vermittlungs- bzw. Beratungsdiensten (Promotionsberater oder andere Personen) in Anspruch genommen wurde sowie keinerlei Dritte vom Doktoranden unmittelbar oder mittelbar geldwerte Leistungen für Tätigkeiten erhalten haben, die im Zusammenhang mit dem Inhalt der vorgelegten Arbeit stehen.

Vera Laurenz

Teile dieser Arbeit wurden bereits an der nachstehend aufgeführten Stelle auszugsweise veröffentlicht.

Laurenz V., Fonseca R.O.C., Ballhaus, C., and Sylvester P.J. (2010) Solubility of palladium in picritic melts: 1. The effect of iron. *Geochimica et Cosmochimica Acta* **74**: 2989–2998.

"Der unermesslich reichen, stets sich erneuernden Natur gegenüber wird der Mensch, soweit er auch in der wissenschaftlichen Erkenntnis fortgeschritten sein mag, immer das sich wundernde Kind bleiben und muss sich stets auf neue Überraschungen gefasst machen."

Max Planck

Contents

List of Tables

List of Figures

Abstract

The highly siderophile elements (HSE – Os, Ir, Ru, Rh, Pt, Pd, Re and Au) are characterized by their highly siderophile and at the same time chalcophile geochemical behavior. As such, they are useful tracers in planetary differentiation processes, as well as processes like partial melting ocurring in the Earths mantle.

An important aspect in HSE geochemistry is their solubility in silicate melts, which is known to depend on different variables such as oxygen fugacity (fO_2), temperature and pressure. To date, experimentally determined HSE solubilities in silicate melt are mostly available for synthetic melt compositions in the CMAS (CaO-MgO-Al_2O_3-SiO_2) system. The most striking differences of these compositions to natural basaltic melts are the absence of Fe-oxides and S. Little is known about the possible effect of Fe-oxides or S on HSE solubility in silicate melts. In the framework of this thesis, the effects of Fe-oxides and S on the solubility of the HSE are investigated experimentally, in order to improve the knowledge on HSE geochemistry.

In the first part of this dissertation, the effect of Fe-oxides on the solubility of Pd in silicate melts is evaluated. The results of experiments are reported, where the solubility of Pd in a natural Fe-bearing picritic melt was investigated as a function of oxygen fugacity (fO_2). Palladium increases from 1.07 ± 0.26 ppm at FMQ-2, to 306 ± 19 ppm at FMQ+6.6 (FMQ = fayalite-magnetit-quartz buffer). At a relative fO_2 of FMQ the slope in log Pd concentration vs. log fO_2 space increases considerably, and Pd concentrations are elevated over those established for CMAS melt compositions. The observed change in slope corresponds to a transition from Pd^{1+} to Pd^{2+}. In the same fO_2 range, the ratio of ferric to ferrous iron increases significantly. Furthermore, at a constant fO_2 of FMQ+0.5 Pd concentrations significantly increase with increasing molar fraction of iron ($X_{FeO-total}$) in the melt. Therefore, we consider ferric Fe to promote the formation of Pd^{2+}. By this the solubility of Pd in the picrite melt is enhanced significantly. The presence of Fe-oxides in the silicate melt has proven to be an important melt compositional parameter. Since most natural melt compositions have substantial Fe-oxide contents, the effects of Fe-oxides should be investigated in future experimental studies.

The second part of this thesis focusses on the effect of sulfur on the solubility of Ru

and Pd in picritic melts. In order to experimentally investigate the effect of S^{2-} on the solubility of HSE in silicate melts, a natural picrite was equilibrated with Ru or Pd metal at 1300 ℃ in a one atm vertical gas mixing furnace under controlled sulfur fugacity (fS_2) and fO_2. Results show that Ru solubility in silicate melts is significantly smaller than the solubility of Pd. Ruthenium solubility in picrite increases from 0.03 ± 0.01 ppm (FMQ) to 3.7 ± 0.7 ppm (FMQ+2), indicating that Ru dissolves as Ru^{4+} in silicate melts.

When S^{2-} is present as a ligand in addition to O^{2-}, Pd concentrations decrease compared to the S-free melt at identical fO_2. The reason is, that Pd-metal readily reacts with the continuously supplied SO_2 of the gas mixture to form an immiscible Pd-dominated sulfide melt. Due to the lower activity of Pd in the sulfide, Pd concentrations in the coexisting silicate melt decrease compared to a S-free melt. In contrast, Ru metal is stable also at high fS_2, and experiments did not exsolve an immiscible sulfide liquid. The solubility of Ru in the picritic melt is enhanced more than one order of magnitude in sulfur-bearing experiments relative to S-free melts at identical fO_2. These results demonstrate that Ru, and possibly other HSE as well, bond with S^{2-} anions, and dissolve as HSE-S species in a silicate melt in addition to their oxide species. Using the $Fe^{3+}/\Sigma Fe$ ratio in the silicate melt to quantify the oxygen available to associate with Ru, the preference of Ru to associate with S^{2-} is calculated to be ~ 1000 times larger than to associate with O^{2-}. This simple estimate clearly shows that sulfur has the major control on Ru solubility in silicate melts, and possibly on the solubilities of other HSE as well.

This result adds towards an improved understanding of HSE geochemistry and their behavior in magmatic systems. It shows that natural basalts should be undersaturated with respect to HSE. Even HSE-rich komatiites have HSE concentrations well below the saturation limit in S-bearing silicate melt. Futhermore, the results provide a mechanism for the enrichment of HSE from a silicate melt into a sulfide liquid. All metal-S molecules including RuS_2 present in the silicate melt are directly sequestered into an exsolving sulfide melt. This mechanism produces a sulfide liquid highly enriched in Ru and other HSE from the onset of sulfide saturation, without the need for complex mixing scenarios.

1 Introduction

The highly siderophile elements (HSE – Os, Ir, Ru, Rh, Pt, Pd plus Re and Au) are a group of elements with similar chemical and physical properties. All HSE have a melting point higher than Fe (1538 ℃). The melting points range from 1555 ℃ (Pd) to 3033 ℃ (Re). At the same time, most of the HSE belong to the group of the noble metals. As such, they are resistant to corrosion or oxidation at room temperature. The reduction potentials of the HSE-oxides are distinctly higher than that of FeO (e.g. O'Neill et al., 1995; Palme, 2008), showing that the HSE-metals are very resistant to oxidation.

Due to their distinct chemical properties, the HSE have gained increasing economic importance. They are invaluable in a variety of technical applications, such as vehicle catalysts and chemical catalysts, electronic components and computer hard discs, fuel cells, glassmaking equipment or medicine. Over the last decade noble metal prices increased dramatically. For example, the price of Pt increased more than fourfold from 474 US$/oz. tr. (1 oz.tr. = 31.1034768 g) in January 2002 to a maximum of 2060 US$ in May 2008 (monthly averages – Johnson Matthey Base Price). Currently (January 2012) Pt is traded with a price of 1510 US$/oz. tr. This price trend is a result of the increasing demand, but also because of the scarcity of the HSE in the accessible part of the Earth. The average HSE abundances in the Earth's upper continental crust are extremely low, with concentrations in the sub-ppb level (Peucker-Ehrenbrink and Jahn, 2001; Rudnick and Gao, 2003, see Table 1). Exploitable enrichments of HSE in the crust (> 1 ppm) are only found in a few ore deposits worldwide, mostly associated with magmatic sulfides (Fig. 1.1). The majority of present-day production is concentrated in South Africa and Russia, with 97 % of the global HSE production.

In Earth Sciences, the importance of the HSE is not only based on their economic importance, but also because of their distinct (geo-)chemical properties. Geochemically, the HSE are classified to be highly siderophile, and at the same time chalcophile elements, due to their strong affinity to partition into metal-rich or sulfide-rich phases (e.g. Borisov and Palme, 2000; Fleet et al., 1999; O'Neill et al., 1995; Peach et al., 1990). These properties make HSE useful tracers of processes where metallic or sulfide phases are involved.

Table 1.1: Overview of HSE abundances in different reservoirs (CI chondrite, primitive upper mantle (PUM) and average crust). All concentrations are given in ng/g (ppb).

	Re	Os	Ir	Ru	Rh	Pt	Pd	Au
CI chondrite[a]	39.5	506	480	683	140	982	556	148
PUM[b]	0.32	3.4	3.2	4.55	0.93	6.6	3.27	0.88
average crust[c]	0.198	0.031	0.022	0.34	–	0.5	0.52	1.5

[a]CI chondrite from Palme and Jones (2003)

[b]PUM from Palme and O'Neill (2003) except Rh, which is from Witt-Eickschen (2003)

[c]Peucker Ehrenbrink and Jahn (2001) except Au which is from Rudnick and Gao (2003)

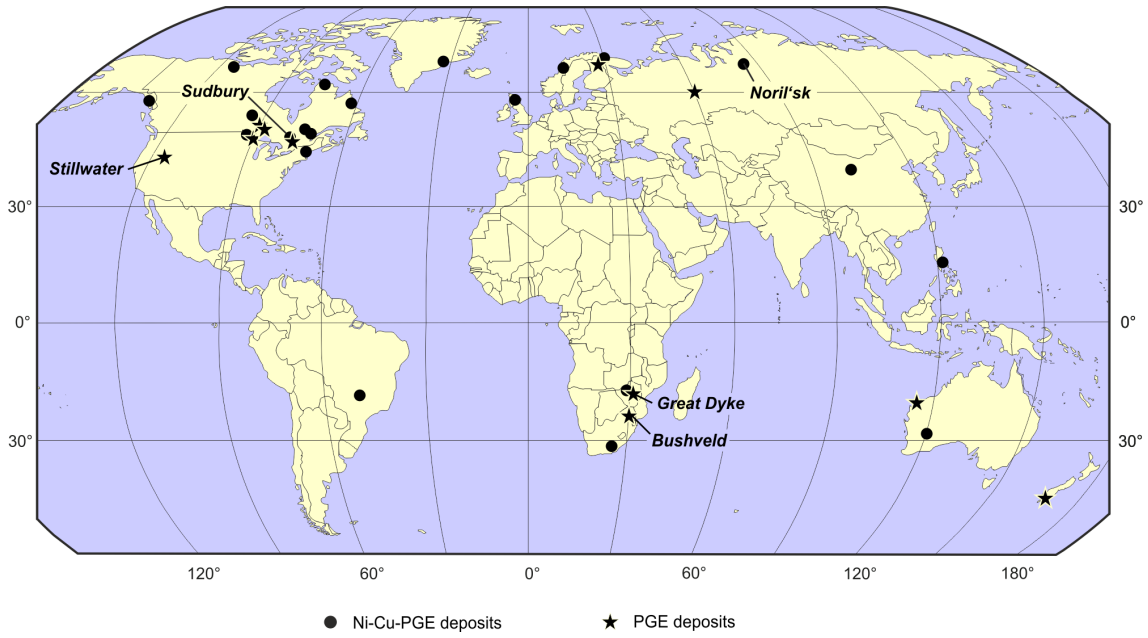

Figure 1.1: Global distribution of the most important magmatic sulfide ore deposits. Stars represent PGE-deposits (PGE = Platinum group elements), whereas circles denote Ni-Cu (-PGE) deposits (after Naldrett, 2004). A few prominent examples are labeled in the map.

1.1 Core formation and the late veneer

Probably the most important process on Earth involving a metallic phase is the differentiation of the Earth and the segregation of its metallic core. Due to their highly siderophile character, the HSE were effectively scavenged from the silicate Earth during the segregation of the metallic core (e.g. Arculus and Delano, 1981; Jagoutz et al., 1979; Ringwood, 1979). With a conservative estimate of their metal-silicate partition coefficients ($D_{\mathrm{HSE}}^{\mathrm{metal-silicate}}$) of $\sim 10^4$ it follows that more than 98%

of the Earth's HSE inventory resides in the core (e.g. McDonough, 2003; Lorand et al., 2008). In turn, the silicate Earth was almost completely devoid of the HSE after core formation was finished.

However, the estimated HSE abundances of the primitive upper mantle (PUM – Table 1) argue against a core-mantle equilibrium. The HSE abundances in PUM are higher by several orders of magnitude than abundances calculated from experimentally determined $D_{\mathrm{HSE}}^{\mathrm{metal-silicate}}$ (e.g.. Borisov and Palme, 2000; Brenan and McDonough, 2009; Cottrell and Walker, 2006; Drake and Righter, 2002; Ertel et al., 2008; O'Neill et al., 1995). Furthermore, the proportions of the HSE among each other are roughly chondritic (Barnes et al., 1985; Crocket, 2002; Lorand et al., 1999; Mitchell and Keays, 1981; Morgan et al., 1981), which cannot be reproduced given the large differences of $D_{\mathrm{HSE}}^{\mathrm{metal-silicate}}$ between the individual HSE ($10^6 - 10^{11}$ – e.g. Borisov and Palme, 2000; Brenan and McDonough, 2009; Mann et al ., in press).

Several hypotheses have been suggested to explain the observed HSE systematics of the Earth's mantle. These include core-mantle interaction (e.g. Brandon et al., 1999; Brandon and Walker, 2005; Snow and Schmidt, 1998), inefficient core formation (e.g. Arculus and Delano, 1981; Jones and Drake, 1986) or heterogeneous accretion (e.g. Newsom, 1990; Ringwood, 1979; Wänke, 1981). Moreover, it has been proposed that higher pressure and temperature lead to lower $D_{\mathrm{HSE}}^{\mathrm{metal-silicate}}$ (Cottrell and Walker, 2006; Murthy, 1991; Righter and Drake, 1997; Righter et al., 2008; Yokoyama et al., 2009). These authors state that the observed HSE abundances in PUM could be reproduced using these lower $D_{\mathrm{HSE}}^{\mathrm{metal-silicate}}$. However, the $D_{\mathrm{HSE}}^{\mathrm{metal-silicate}}$ of all HSE differ by at least one to two orders of magnitude at equal pressure-temperature conditions (e.g. Brenan and McDonough, 2009; Mann et al., in press), underlining that the HSE should have been fractionated from each other by high temperature-high pressure equilibrium partitioning during formation of the Earth's core.

Probably the most widely accepted model explaining the observed HSE systematics of the Earth's mantle is the so-called late veneer model (e.g. Chou, 1978; Kimura, 1974; Morgan et al., 1981, 2001; O'Neill, 1991). In this model, a certain amount of chondritic material was added to the silicate Earth after core formation was complete. This material was well mixed into the mantle, replenishing the HSE inventory of the mantle, and imposing the observed chondritic ratios. Up to 0.4% of the total mass of the Earth was added by the late veneer (Morgan et al., 2001). Please note, that recent

estimates of the PUM composition point towards non-chondritic HSE abundances, requiring a modification of the late veneer hypothesis (Becker et al., 2006). Also, the HSE systematics of mantle peridotites may have been overprinted by widespread refertilization (e.g. Luguet et al., 2008; Lorand et al. 2010). Therefore, the current estimates of PUM should be considered as "work in progress" (Lorand et al., 2008).

1.2 Fractionation of the HSE during partial melting of the mantle

In general, the HSE are transported from the mantle to the crust by partial mantle melts. There are remarkable differences in the behavior of the individual HSE during partial melting. Average mantle normalized HSE-patterns of basalts from different tectonic settings all reveal that the HSE are fractionated from each other (Crocket, 2002; see Fig. 1.2). The HSE with lower melting points (Pd, Pt, Re and Au) are sequestered to the partial melt, while Os, Ir and Ru are retained in the residue (e.g. Barnes et al., 1985, 1988; Pearson et al., 2004; Philipp et al., 2001). The only exception is Re, which behaves incompatible (Fonseca et al., 2007; Mallmann et al., 2007), despite its high melting point of 3033 ℃.

There is consensus, that sulfides play a major role for the behavior of the HSE during mantle melting, because the HSE budget of the Earth's mantle is dominated by mantle sulfides (e.g. Alard et al., 2000; Bockrath et al., 2004a; Handler and Bennett, 1999; Lorand et al., 2008; Luguet et al., 2003, 2004, 2008; Mitchell and Keays, 1981). The upper mantle typically contains 0.1 vol.% base metal sulfides, with measured HSE concentrations in the ppm-level. Hence, more than 90 % of the HSE budget of mantle lherzolites resides in base metal sulfides (Alard et al. 2000; Hart and Ravizza, 1996; Lorand and Alard, 2001; Lorand et al., 2008).

Therefore, the behavior of the HSE is closely linked to the behaviour of the sulfides that host them. However, simple equilibia between sulfide melt and silicate melt alone cannot explain the observed fractionation among the HSE (cf. Ballhaus et al., 2006 and references therein). As a solution to this problem, it has been suggested that a crystalline phase must be present in the mantle in addition to sulfide liquid, which retains Os, Ir and Ru.

Indeed, two different populations of sulfide have been identified in mantle lherzolite: Interstitial , and Os-, Ir- and Ru-rich monosulfide solid solution (mss) enclosed in

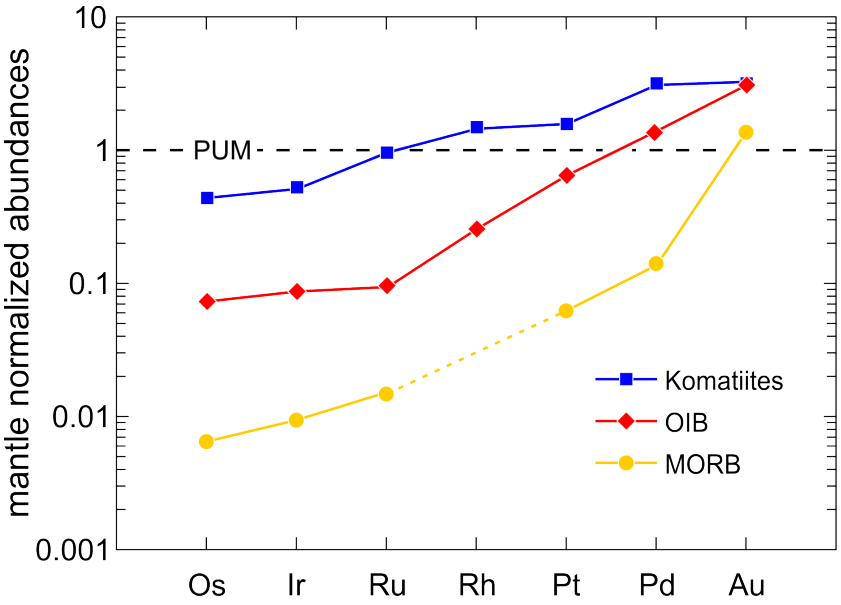

Figure 1.2: Average mantle normalized HSE abundances in basalts from different tectonic settings (Crocket, 2002). PUM – primitive upper mantle (Palme and O'Neill, 2003).

silicates (e.g. Alard et al., 2000; Harvey et al., 2011; Lorand and Alard, 2001; Mungall and Su, 2005; Pearson et al., 2002). The existence of two populations of sulfide (i.e. mss and sulfide melt) due to incongruent melting of mantle sulfides was confirmed experimentally by Bockrath et al. (2004a). Furthermore, mss is known to concentrate Os, Ir and Ru, while Pt and Pd partition into a coexisting sulfide liquid (Ballhaus et al., 2001, 2006). During partial melting crystalline mss is trapped in the residuum, retaining Os, Ir, and Ru. The Pt- and Pd-rich Cu-Ni-sulfide is entrained in the silicate melt. The HSE may then either be carried to the crust as HSE-sulfide droplets in suspension (Ballhaus et al., 2006; Bockrath et al., 2004a), or as oxide or sulfide species dissolved in the silicate melt.

Other possible phases potentionally fractionating the HSE are laurite (RuS_2), chromites or Os-, Ir-, and Ru-rich alloys (Ballhaus et al., 2006; Bockrath et al., 2004b; Brenan et al., 2011; Fonseca et al., 2011; Luguet et al.; 2003). Such alloys can precipitate from mantle sulfides as a result of the extraction of sulfur with progressive melting (Luguet et al., 2007; Fonseca et al., 2011). Other researchers attribute their formation to an oversaturation of a silicate melt with respect to HSE-metal (e.g. Barnes and Fiorentini, 2008; Borisov and Palme, 2000; Tredoux et al., 1995). The solubility of HSE in natural silciate melts is the key parameter, since exceeding solubility causes oversaturation with respect to HSE-metal.

1.3 Enrichment of HSE in magmatic sulfides

Most of the known HSE enrichments in the crust are associated with sulfides found in mafic layered intrusions (e.g. Merensky Reef, Bushveld Complex; JM Reef, Stillwater Complex). In principle, most mafic magmas contain sufficient amounts of HSE to be a potential source magma for the formation of an ore body (Simon and Ripley, 2011). In general, HSE-rich magmas favour the formation of HSE-rich ore deposits. These can be generated by high degrees of partial melting ($\sim 25\,\%$), where all S is extracted from the mantle and the HSE hosted by sulfides are liberated (e.g. Keays, 1995). Alternatively, the consumption of sulfur can also be achieved if melting takes place under oxidizing conditions where sulfate is stable. The solubility of sulfate in silicate melt is an order of magnitude higher than that of sulfide (e.g. Caroll and Rutherford, 1985; Jugo et al., 2005; Jugo, 2009). Under oxidizing conditions applicable to the formation of many arc magmas (fO_2 = FMQ+1.7), 6% of partial melting is sufficient to consume all HSE-bearing sulfides of the source, and to generate HSE-rich magmas (Jugo, 2009).

The enrichment of HSE to an economically exploitable ore is then closely related to the exsolution of a FeS-rich sulfide melt from a silicate melt. The HSE are concentrated in the exsolving immiscible sulfide droplets, because of the chalcophile character of the HSE (e.g. Fleet et al., 1999; Peach et al., 1990). HSE concentrations in a sulfide melt are at least four orders of magnitude higher than in the coexisting silicate melt. For example, sulfides of the Merensky Reef (Bushveld Complex, cf. Fig. 1.1) contain around 500 ppm ΣHSE, whereas ΣHSE in the parental melt is only 20–30 ppb (Fig. 1.3).

At shallow depth, magmas are generally sulfide-undersaturated, as sulfide capacity at sulfide saturation (SCSS) increases strongly with decreasing pressure (O'Neill and Mavrogenes, 1999). Therefore, sulfide saturation must be triggered in order to concentrate the HSE. Different mechanisms esist to cause sulfide saturation of a basaltic melt. The most important ones are the assimialtion of S-rich countryrock, low-pressure fractional crystallization, or a combination of both (e.g. Mungall and Naldrett, 2008 and references therein). The resulting immiscible sulfide melt will be highly enriched in the chalcophile HSE.

A popular model that is often used to quantify HSE enrichment in sulfide melt is the R-factor model of Campbell and Naldrett (1979). This model suggests that the

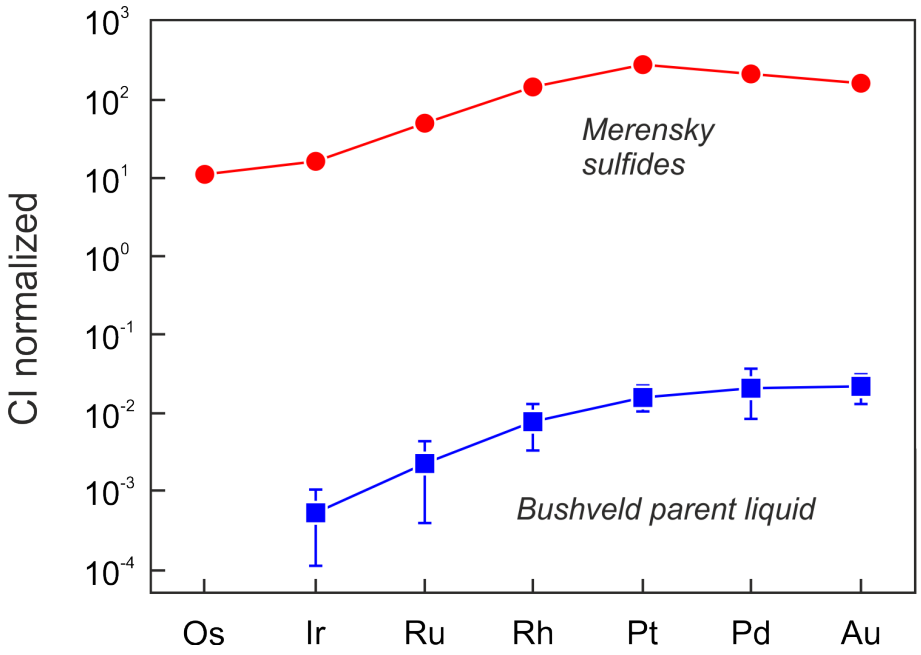

Figure 1.3: HSE abundances of sulfides from the Merensky Reef, Bushveld complex (Naldrett et al., 1986) and the parent liquid (Davies and Tredoux, 1985) normalized to CI chondrite (Palme and Jones, 2003). The sulfides are enriched 10,000-fold relative to their parental magma, which is a result of the extreme preference of the HSE to partition into the sulfide phase.

level of HSE enrichment in sulfides is controlled by the mass ratio between sulfide melt and silicate melt. However, it is still poorly understood how the HSE are transferred from silicate to sulfide liquid. Campbell et al. (1983) suggested that magma chamber turbulences enable immiscible sulfide droplets to equilibrate with a large volume of silicate melt, scavenging the HSE after sulfide exsolution. However, this suggestion remains controversial because of contrasting field evidence (e.g. Ballhaus and Ryan, 1995; Ballhaus and Sylvester, 2000). In this context, the solubility of the HSE in silicate melts, namely if they dissolve as oxide or sulfide species, can help to better understand the mechanisms for HSE enrichment in magmatic sulfides.

1.4 Solubility of the HSE in silicate melts

As stated above, the solubility of the HSE, and the variables controlling it, is a key aspect that has been target of investigation. The solubility of the HSE in silicate melts is critical for understanding their geochemical behavior. There have been numerous experimental studies where the solubility of the different HSE in silicate melt has been investigated at one atm total pressure (Borisov et al., 1994; Borisov

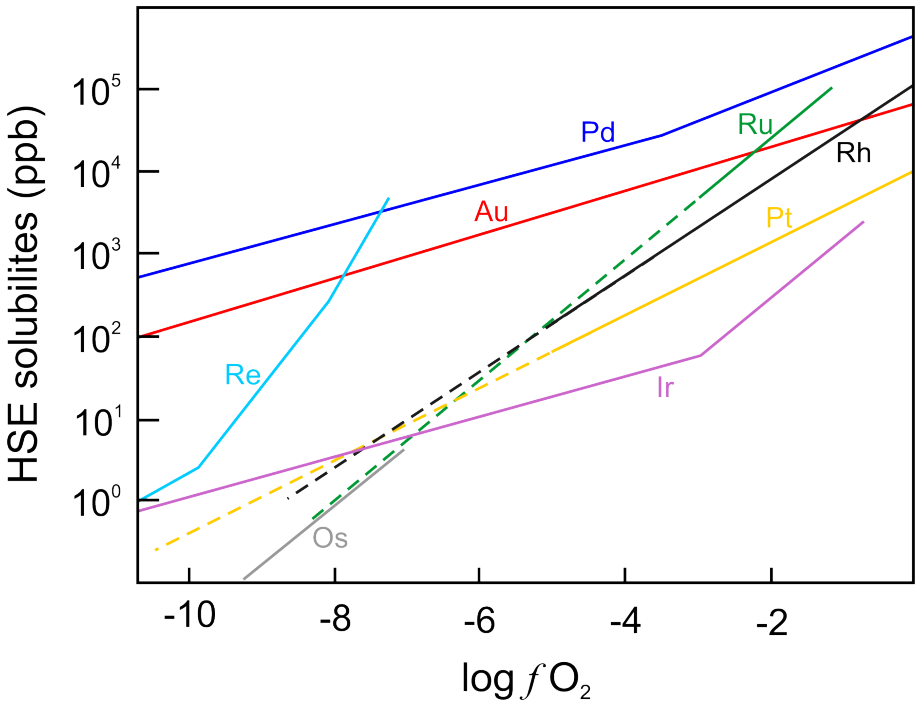

Figure 1.4: Experimentally determined solubility of the different HSE in Fe-free silicate melts as function of fO_2 at 1300 °C (modified from Ertel et al. 2008; Walter et al.,2000). Solid lined represent experimentally determined solubilities (Borisov et al., 1994; Borisov and Nachtweyh, 1998; Borisov and Palme, 1995, 1996; Ertel et al. 1999, 2001; Fortenfant et al., 2003, 2006;). Dashed lines indicate extrapolations of the solubilities to lower fO_2 values.

and Palme, 1995, 1997, 2000; Capobianco et al., 1993; Ertel et al., 1999, 2001, 2008; Fortenfant et al., 2003, 2006; Jones and Drake, 1986; O'Neill et al., 1995). Overall, the solubility of the HSE in silicate melts is extremely low. The solubilities of the different HSE in silicate melts are significantly distinct from each other. For example at an fO_2 of FMQ (at 1300 °C) 3.5 ppm Pd can be dissolved in synthetic CMAS (CaO-MgO-Al_2O_3-SiO_2) silicate melts (Borisov et al., 1994), whereas only 2.5 ppb Pt can be dissolved (Ertel et al., 1999). These studies have shown that the solubility of the HSE in silicate melt is mainly controlled oxygen fugacity (fO_2) and to a lesser extent by temperature. These results indicate that the HSE dissolve as oxides in silicate melts (Fig.1.4).

The oxidation state of an element can be derived from its fO_2 dependending solubility (cf. chapter 2.1 and 3.2). While the details regarding the valence states of the HSE differ between the individual studies, it was generally observed that the HSE dissolve in unusually low oxidation states in CMAS melts (e.g. O'Neill et al., 1995; Borisov and Palme, 2000). Palladium, Ir and Au were found to be predominantly

univalent over a wide range of fO_2 relevant for the Earth's mantle, while Pt dissolves as Pt^{2+} (Borisov et al., 1994; Borisov and Palme, 1995, 1996, 1997, 2000; Ertel et al., 1999). All these formal valences are lower than what was known from the most stable oxides of the respective elements (e.g. Ir^{4+} in IrO_2).

1.4.1 The nanonugget problem

The analysis of HSE concnetrations has proven to be challenging, due to their very low concentrations in experimentally produced glasses. In many of the pioneering studies (e.g. Borisov et al., 1994; O'Neill et al., 1995) HSE concentrations were measured using Instrumental Neutron Activation Analysis (INAA). Because INAA is a bulk analytical technique, it was not possible to detect small-scale heterogeneities in the glasses. With the development of Laser Ablation Inductively Coupled Plasma Mass Spectrometry (LA-ICP-MS) it became possible to analyze experimental charges *in situ* with high spatial resolution. Using LA-ICP-MS, it became obvious that small-scale heterogeneities in the HSE distribution (so-called nanonuggets) are ubiquitously present in experimental HSE-bearing glasses (e.g. Brenan et al., 2003; Ertel et al., 2001, 2008; Fortenfant et al., 2006).

Whether these nanonuggets form upon quenching (e.g. Cottrell and Walker, 2002, 2006), or if they are already existing at run conditions (e.g. Ertel et al., 2008) is still a subject of debate. This issue is of vast importance for the determination of HSE solubilites. If nuggets were indeed the result of exsolution of metal that was originally dissolved in the silicate melt (presumably at zero valence state), then the nuggets would have to be included when calculating HSE concentrations from LA-ICP-MS spectra. On the other hand, if nanonuggets are present at run conditions, spikes in the time resolved laser spectra need to be removed from the laser spectra to obtain "true" concentrations. Whether or not the nuggets are included lead to order of magnitude differences in metal-silicate partition coefficients for the HSE (Ertel et al., 2008). However, it appears to be unrealistic that metals in zero valence state may dissolve in a silicate melt dominated by oxide components. In a recent study Medard et al. (2010) performed experiments to investigate Pt solubility in natural basaltic melt using a centrifuging piston-cylinder aparatus (Schmidt et al., 2006). The silicate glasses of these dynamic experiments are free of nanonuggets, in contrast to static experiments (i.e. not centrifuged). Therefore, Medard et al. (2010)

concluded that nanonuggets are present at run conditions, and need to be excluded when determining HSE solubilities in silicate melts.

It is therefore necessary to complement INAA determined HSE solubilities with additional studies using LA-ICP-MS. This should result in more reliable solubility data and in accurately determined oxidation states.

1.4.2 The effect of melt composition

Despite the large amount of experimental data on HSE solubilities in silicate melts, the effect of melt composition is largely unknown. It has become evident in recent years that melt composition may have an important effect on the behavior of trace elements in magmatic systems (e.g. Borisov and Danyushevsky, 2011; Kohn and Schofield, 1994; O'Neill and Eggins, 2002; Rose-Weston et al., 2009; Yana and Walker, 1997b). For example, the solubility and oxidation state of Mo depends on the abundance of CaO in the melt (O'Neill and Eggins, 2002). Variations in major and trace element composition may also affect the solubility of the HSE in silicate melts. In a recent study, Borisov and Danyushevsky (2011) have shown that the solubility of Pt and Rh in their silicate melt is inversely correlated with the SiO_2 content of the melt (i.e. the degree of polymerization), although Pd solubility shows little change over the same range in SiO_2.

However, most of the previous studies investigating HSE solubilities were carried out using synthetic melt compositions as an analog to basaltic melts. Mostly, compositions in the CMAS system were used, because they are easier to handle experimentally than natural compositions. One of the most striking differences to natural basaltic melts is the absence of Fe-oxides. It was assumed that the presence or absence of Fe-oxides in silicate melts does not change the activity of the HSE in silicate melts (Borisov and Palme, 2000; O'Neill et al., 1995). Borisov et al. (2000) theoretically assessed the effect of Fe on HSE solubility in a silicate melt, by considering the activity composition relations in the various Fe-HSE binary systems. The solubilities of the different HSE should decrease because the activities of the HSE in HSE-Fe alloys are lower compared to the pure HSE metal. However, the possible effect of Fe-oxides as a silicate melt component remains largely unknown, because experimental data are missing.

Likewise, little is known about the possible effect of S on HSE solubility even

though the HSE are known to be chalcophile. In particular, little is known about the possible effect of sulfur fugacity (fS_2) on the solubility of HSE in silicate melts, i.e. the role of S^{2-} as possible ligand for the HSE. The influence of sulfur on HSE solubility in silicate melts is typically regarded as being unimportant due to thermochemical arguments (e.g. Fonseca et al. 2009; O'Neill et al., 1995; Tuff and O'Neill, 2010). It has been argued that the effect of S^{2-} on the activity of the HSE-oxide species in silicate is negligible since the abundance of oxygen in silicate melts (~ 45 wt.%) is orders of magnitude higher than that of sulfur (~ 1000 ppm).

However, experimental studies have shown that Pt and Pd are strongly associated with ligands such as Te (Helmy et al., 2007) and As (Helmy et al., 2010). Given that As, Te and S are chalcogenes, it is likely that HSE dissolve in silicate melts in association with S^{2-}. Indeed, recent studies indicate that S^{2-} in silicate melt may act as a ligand for chalcophile elements. Based on a negative correlation between $D_{\mathrm{Ni}}^{\mathrm{olivine-silicatemelt}}$ and S concentrations in mid-ocean ridge basaltic (MORB) glasses, Li et al. (2003) suggested that Ni and S interact to form Ni-S complexes in silicate melts. Since HSE are more chalcophile than Ni, the effect of S on their solubility in silicate melt is probably even more pronounced (Naldrett et al., 2008). In contrast, Tuff and O'Neill (2010) have shown that there is only little effect of S^{2-} on Ni partitioning between olivine and silicate melt. However, recent experimental results were interpreted to indicate the formation of Mn-S (Evans et al., 2008) or Re-S (-O) associations in silicate melts (Brenan, 2008). Furthermore, experimental studies on the solubility of Au in silicate melts indicate that the presence of S enhances Au solubility in the melt (Botcharnikov et al., 2011; Jégo et al., 2010; Jégo and Pichavant, in press). If the HSE are associated with S in silicate melts to form HSE-S compounds, this will have implications for the presumed mechanisms of the formation of magmatic sulfide HSE-deposits, as well as on how the HSE behave during partial melting of the upper mantle.

As outlined above, the composition of the silicate melt is an important variable controlling the solubility of the HSE. This thesis therefore focusses on the effects of melt composition on HSE solubility in silicate melts. In particular, the effect of Fe-oxides and sulfur on Pd and Ru solubility are investigated experimentally, and HSE concentrations are determined by LA-ICP-MS. In chapter 2 the effect of Fe-oxides on Pd solubility is investigated. A redox-exchange between Fe- and Pd- oxide species is proposed, which increases Pd-solubility in silicate melts. Chapter 3 focusses on

the effect of S on Ru and Pd solubility in picritic melt, showing that sulfur has the major control on HSE solubility. The implications for saturation of silicate melts with HSE-rich alloys are discussed, and a new mechanism for the formation of HSE-rich sulfides is presented.

2 Solubility of Pd in picritic melts: The effect of iron

2.1 Introduction

The highly siderophile elements (HSE – Pt, Pd, Rh, Os, Ir, Ru, Re and Au) are among the rarest and most valuable elements found on Earth. Not only are they useful in tracing processes such as core-mantle differentiation (e.g. Chou, 1978; Kimura et al., 1974; O'Neill et al., 1991; Righter et al., 2008) and possible core-mantle interaction (e.g. Brandon et al., 1999; Brandon and Walker, 2005; Puchtel et al., 2005); they are also key to understanding processes within the Earth's mantle, including partial silicate melting (e.g. Barnes, 1985; Pearson et al. 2004; Phillip et al., 2001), melt segregation (Bockrath et al., 2004a), and mantle metasomatism (e.g. Alard et al., 2005; Becker et al., 2001; Lorand et al., 2008; Luguet et al., 2008).

The primary reservoir for the HSE is the Earth's mantle. Estimates of total HSE in primitive upper mantle (PUM) range from 23 to 32 ppb (e.g. Becker et al., 2006; Palme and O'Neill, 2003). The transport of the HSE from the mantle to the crust is via primitive silicate mantle melts, either as oxide and sulfide species dissolved in silicate melt (e.g. Borisov and Palme, 2000) or as HSE-bearing sulfide melt droplets in suspension in a silicate melt (Ballhaus et al., 2006; Bockrath et al., 2004a; Fonseca et al., 2009). In order to discriminate between these transport modes, it is essential to evaluate how and to what extent the HSE are dissolved in silicate melt.

Previous experimental studies (Borisov et al., 1994, 2004; Borisov and Palme, 1995, 2000; Capobianco et al., 1993; Capobianco and Hervig, 1996; Cottrell and Walker, 2006; Ertel et al., 1999, 2001, 2008; Fortenfant et al., 2003, 2006; O'Neill et al., 1995; Righter et al., 2008; Yokoyama et al., 2009) have shown that the HSE are dissolved in silicate melts as oxide species, according to

$$M^{alloy} + \frac{x}{4}O_2 \Leftrightarrow MO_{x/2}^{silicate} \tag{2.1}$$

where x is the valence state of the metal M in the silicate melt. One of the principal variables in controlling HSE solubility is the oxygen partial pressure (fO_2). The

activity of the HSE oxide species in solution in silicate ($a^{\text{silicate}}_{\text{MO}_{x/2}}$) is given by

$$\log a^{\text{silicate}}_{\text{MO}_{x/2}} = \log K + \log a^{\text{alloy}}_{\text{M}} + \frac{x}{4}\log fO_2 \tag{2.2}$$

and may be calculated if the equilibrium constant K and the activity-composition relations for both metal and oxide species in solution are known. Assuming that HSE dissolution in silicate melt is ideal, the activity coefficient ($\gamma^{\text{silicate}}_{\text{MO}_{x/2}}$) is unity. For constant melt compositions the valence state of the HSE cationic species can then be derived from the slope (m) of the concentration profile in log-concentration vs. log fO_2 space, where the valence is given by

$$m = \frac{x}{4} \tag{2.3}$$

Solubilities of the HSE in silicate melts at one atm have mostly been determined in synthetic anorthite-diopside (AnDi) eutectic melt compositions (e.g. Borisov et al., 1994; O'Neill et al., 1995). However, many authors regard this system to be too simplistic (e.g. Hillgren et al., 1996; O'Neill and Eggins, 2002; Rose-Weston et al., 2009) and melt composition (i.e. CaO, MgO, FeO or S concentrations, degree of polymerization) has been shown to be an important factor for the solubility of trace elements in silicate melts at sulfide-undersaturated conditions. This raises the question if, and to which extent, melt components such as FeO and S^{2-} also influence HSE solubility.

Borisov et al. (2000) considered the effect of Fe in the metal phase on HSE solubility in silicate melts by applying the activity-composition relations for Fe-HSE alloy systems to calculate the concentrations expected in natural Fe-bearing magmas. These authors stated that metallic Fe alloying with Pd will lower Pd concentration in AnDi melts, however, they downplayed possible interactions of ferrous and ferric iron species with Pd oxide species within the silicate melt. Very little experiments are available to judge if dissolved S^{2-} affects the solubility of HSE; however, O'Neill et al. (1995) argued that the effect must be small because the S^{2-} anionic ligand is about 200 times less abundant in a basaltic silicate melt than the O^{2-} ligand.

In this contribution, we investigate the effect of FeO and $FeO_{1.5}$ on Pd solubility in silicate melt. We report experiments with FeO-bearing picritic melt in Pd wire loops over a range in relative fO_2 from FMQ−2 to FMQ+6.6 (FMQ = fayalite-magnetite-

quartz buffer, as calibrated by O'Neill et al., 1987). All Pd concentrations in silicate were measured by Laser Ablation Inductively Coupled Plasma Mass Spectrometry (LA-ICP-MS). Owing to its spatial resolution LA-ICP-MS allows the distinction between HSE in solution (cf. Eq. 2.1) and HSE present as micro-nuggets, unlike Instrumental Neutron Activation Analysis (INAA) which is a bulk analytical technique (cf. Ertel et al., 2006, 2008). We show that iron oxide species play a major role in controlling the solubility of Pd in silicate melt. Not only does Fe dilute the activity of Pd in the Pd-Fe alloy phase as predicted by Borisov and Palme (2000), FeO and $FeO_{1.5}$ species in the silicate melt undergo redox exchange reactions with dissolved $PdO_{x/2}$ species, tending to raise Pd solubility in silicate relative to iron oxide-free silicate melts.

2.2 Experimental procedures

Solubility experiments were carried out in a one atm vertical muffle tube furnace equipped for gas mixing. The starting silicate melt composition is a natural picritic basalt with $\sim$12 wt.% MgO, henceforth picrite, from the Solomon Islands (SE1 – Rohrbach et al., 2005; Schuth et al., 2004). We employed the wire-loop technique where the picrite powder is placed in a Pd wire loop, suspended in the hot zone of the furnace, and equilibrated at 1300 °C with a CO–CO_2 ($\pm$ O_2) gas atmosphere (cf. Fig. 2.1). After a run time of 48 hours, experiments were quenched in air by quickly drawing the Pd loop to the water-cooled top of the furnace which is at $\sim$100 °C. Selected experiments were reversed by equilibrating initially Pd-free picrite and picrite doped with PdO in the thousands of ppm concentration range, simultaneously in the same atmosphere. Temperature (1300 $\pm$ 2 °C) was controlled by a Type B thermocouple ($Pt_{94}Rh_6$–$Pt_{70}Rh_{30}$) and calibrated against the melting points of Au and Cu.

Oxygen partial pressure was imposed by CO-CO_2 ($\pm$ O_2) gas mixtures (Chase, 1998). Thermodynamically calculated O_2 partial pressures were checked with a CaO–Y_2O_3-stabilized ZrO_2 solid electrolyte cell and were found to be accurate to within 0.2 log-bars of the calculated fO_2 values. Above a relative fO_2 of FMQ+1, however, precision deteriorates because the amount of CO added to the gas becomes too small to be controlled precisely with our gas flow meters. This problem is circumvented by adding O_2 to the reactant gas. Because O_2 reacts with CO to form CO_2, this

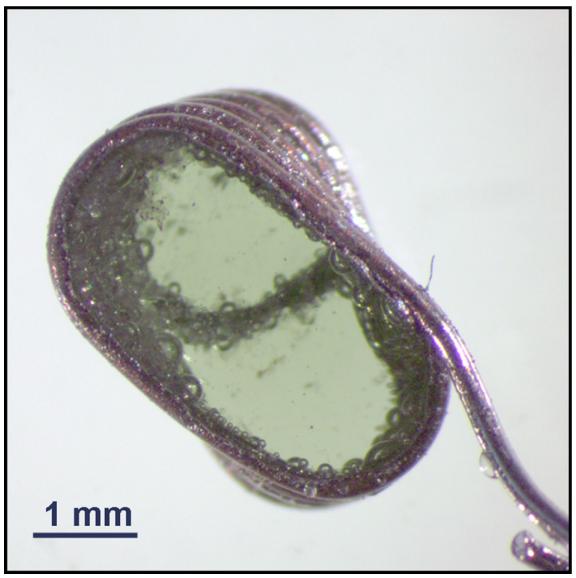

Figure 2.1: Example of a quenched loop experiment. Picrite quenched to a clear green glass and attached to the Pd wire loop.

technique allows CO flow rates well inside the calibration range of the CO flow meter, without actually increasing pCO in the gas mix. With this technique, we can comfortably access fO_2 regions at 1300 °C as high as FMQ+5 (cf. Fig. 2.2). A drawback is that fO_2 can no longer be calculated thermodynamically because if the variable to be calculated is added as a component, the system is overdetermined. However, as fO_2 can be measured independently with a solid electrolyte cell, this is not an issue.

2.3 Analytical procedures

Experimental run products (wire loop and the silicate glass) were analyzed for their major element compositions with a JEOL JXA 8900 electron microprobe analyzer (EMPA) in wavelength dispersive mode (WDS) with an accelerating voltage of 15 kV and a beam current of 15 nA. Standards used were natural silicates and oxides for glass analysis, and pure Pd and Fe for the analysis of the metals. Glasses were analyzed with the beam defocused to 10 µm and metals with a focused beam. Counting times were 10 s on peak and 5 s on background, except for Na and K, which were measured with 5 s and 2.5 s respectively in order to avoid alkali migration. Matrix corrections were done with the ZAF correction method. To check for homogeneity we analyzed up to 15 points randomly distributed on each glass and metal No inhomogeneities were detected. Average compositions are compiled in Table 2.1.

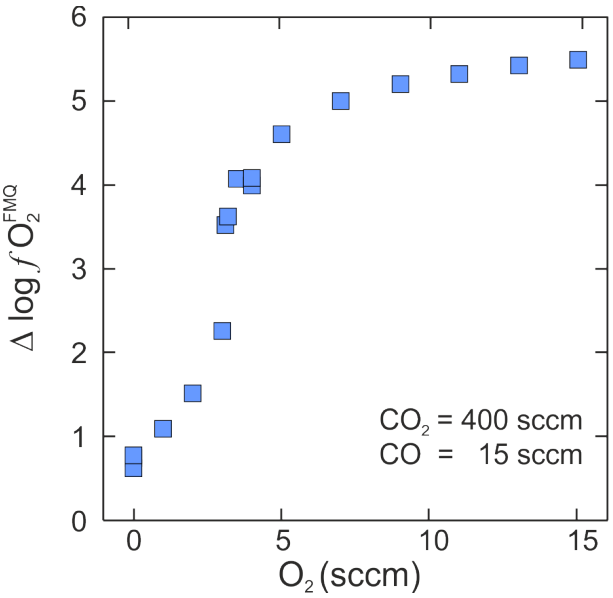

Figure 2.2: Variation in relative fO_2 imposed by the addition of increasing amounts of O_2 to a CO-CO_2 gas mixture. Flow rates of CO and CO_2 held constant at 15 and 400 sccm (standard cubic centimeters per minute), respectively. Oxygen partial pressures were measured in-situ with an Y-stabilized Zirconia cell and are given relative to FMQ (O'Neill, 1987). Errors are smaller than symbol size. Note that the measured fO_2 does not match the fO_2 calculated according to the NIST-JANAF tables, for reasons not evaluated yet.

Palladium concentrations for the silicate glass charges were determined at the Inco Innovation Centre, Memorial University (MUN, New Foundland) using a GeoLas Pro laser ablation system coupled with a Finnigan Element XR inductively coupled plasma-mass spectrometer. The GeoLas system consists of a Lambda Physik COMPexPro 110 ArF excimer laser operating at a wavelength of 193 nm and a pulse width of 20 ns, a beam delivery and ablation cell apparatus, a camera for sample viewing and dedicated software for controlling ablation parameters. Polished samples were placed in an air tight chamber and ablated in helium gas, which increases analyte sensitivities by enhancing sample transport from the ablation cell during deep ultraviolet ablation. Analyses were made on a 40-micron spot with a laser fluence of 5 J/cm^2 and repetition rate of 10 Hz. Data were collected in time-resolved mode with 30 s measurement of the pure gas background, followed by 60 s of measurement during laser ablation. Count rates were measured using one point per peak for each of the following isotopes: ^{25}Mg, ^{27}Al, ^{29}Si, ^{43}Ca (used for internal standardization with Ca values by EPMA), ^{44}Ca, ^{65}Cu, ^{66}Zn, ^{68}Zn, ^{89}Y, ^{92}Zr, ^{105}Pd, ^{106}Pd, ^{108}Pd, and ^{111}Cd. Count rates for ^{65}Cu, ^{66}Zn, ^{68}Zn, ^{89}Y, ^{92}Zr, and ^{111}Cd were monitored for potential isobaric interferences of ^{40}Ar^{65}Cu and ^{89}Y^{16}O on ^{105}Pd; ^{40}Ar^{66}Zn, ^{90}Zr^{16}O

and ^{106}Cd on ^{106}Pd; and ^{40}Ar ^{68}Zn, ^{92}Zr^{16}O and ^{108}Cd on ^{108}Pd; but were found to be negligible in all cases.

Raw data were reduced using the macro-based spreadsheet program LAMTRACE (written by S.E. Jackson; cf. Van Achterbergh et al., 2001) for gas background subtraction, ablation interval selection and concentration calculation. In rare cases where the time-resolved data showed spikes in Pd signal, presumably due to the presence of metal nano-nuggets in the silicate glass, ablation intervals showing no spikes were selected for concentration calculations. A detailed description is given by Ertel et al. (2006). By carefully choosing the integration limits avoiding nano-nugget influenced portions of the spectra, and due to the good spatial resolution of the method, we were able to determine real Pd solubilities.

Concentrations for Pd were calculated for each of the three measured isotopes (^{105}Pd, ^{106}Pd, ^{108}Pd) by external calibration against an in-house synthetic silicate glass standard (synthesized by Holzheid et al., 2000) with a matrix composition of 50.1 wt.% SiO_2, 14.24 wt.% Al_2O_3, 9.66 wt.% MgO, 24.75 wt.% CaO and containing 131 ppm Pd (as calibrated by solution-ICPMS). The calibration standard was run in duplicate before and after a series of 7 to 16 of the unknowns. Each glass charge was analyzed on three to five spots. Reported values for each spot are averages of the results for the three Pd isotopes. NIST 612 reference material was run as an unknown throughout the experiments and the measured values for Pd (1.04 ± 0.12 ppm) compared favorably to the preferred value (1.09 ± 0.09 ppm, Sylvester et al., 1997). To check that Pd metal and silicate glass were homogeneous, hence verify that equilibrium was reached, up to 15 points were randomly distributed across each polished glass shard, and line profiles were run across Pd metal wires. No major compositional inhomogeneities were detected, neither in the silicate nor in the Pd-Fe metal alloys. Forward and reverse experiments were also found to be identical in major element composition and Pd concentration, so it is assumed that redox equilibrium was generally achieved.

2.4 Results

The silicate melt quenched to glasses with a light green color at low fO_2 and brownish colors above FMQ+2 (Fig. 2.1). Some runs at low fO_2 crystallized minor olivine, as confirmed by EPMA, usually found attached to the Pd-wire loop. Nuggets were not

found to be a problem because analysis by LA-ICP-MS, however, provides means of discriminating between Pd dissolved in silicate and Pd in metallic nuggets (e.g. Ertel et al., 2008; Medard et al., 2010).

2.4.1 Metal-silicate melt equilibria with iron

Fig. 2.3 shows the redox net transfer between Fe in the Pd metal and iron oxide species in the silicate melt. The compositional parameter, i.e. $2\log(X_{\mathrm{FeO}}^{\mathrm{silicate}}/X_{\mathrm{Fe}}^{\mathrm{metal}})$ chosen is derived from the the iron-wüstite (IW) equilibrium, i.e.

$$2\mathrm{Fe} + \mathrm{O_2} \Leftrightarrow 2\mathrm{FeO} \tag{2.4}$$

and variations in $2\log(X_{\mathrm{FeO}}^{\mathrm{silicate}}/X_{\mathrm{Fe}}^{\mathrm{metal}})$ are shown versus experimental $f\mathrm{O_2}$ (Fig. 2.3). The fraction of ferrous iron (FeO) in the silicate melt is calculated using the formalism given by Killinc et al. (1983), however, in order to illustrate as to how much iron-oxide may be present as ferric iron ($\mathrm{FeO_{1.5}}$), the diagram is contoured with respect to molar $(\mathrm{Fe^{3+}}/\Sigma\mathrm{Fe})\times 100$ isopleths.

In the $f\mathrm{O_2}$ range covered (FMQ−2 to FMQ+6.6), $2\log(X_{\mathrm{FeO}}^{\mathrm{silicate}}/X_{\mathrm{Fe}}^{\mathrm{metal}})$ varies by eight orders of magnitude. At a relative $f\mathrm{O_2}$ of FMQ (Fig. 2.3) we note a gradual change in slope in $2\log(X_{\mathrm{FeO}}^{\mathrm{silicate}}/X_{\mathrm{Fe}}^{\mathrm{metal}})$. This may indicate that above FMQ, increases with relative $f\mathrm{O_2}$ at a rate faster than in the reduced region below FMQ, as predicted by the Killinc et al. (1983) formalism. In the highly oxidized region above FMQ+4, the Pd metal phase is practically Fe-free (< 0.05 wt.%). Therefore, uncertainties in $2\log(X_{\mathrm{FeO}}^{\mathrm{silicate}}/X_{\mathrm{Fe}}^{\mathrm{metal}})$ become substantial and any possible variations in $2\log(X_{\mathrm{FeO}}^{\mathrm{silicate}}/X_{\mathrm{Fe}}^{\mathrm{metal}})$ in that $f\mathrm{O_2}$ range are within the error bars.

Table 2.1: Experimental conditions and major elements of the glasses and metal as well as the Pd concentrations obtained by LA-ICP-MS.

sample	PD1	PD2	PD3	PD4	PD5[a]	PD6[a]	PD7[a]	PD8[a]
$\Delta \log pO_2^{FMQ}$	−2	−1.4	−1	−0.5	−0.5	−1	−1.4	−2
$CO/CO_2/O_2$ (sccm)	180/288/0	74/240/0	54/280/0	17/154/0	17/154/0	27/140/0	37/120/0	60/96/0
Glass:	wt.% oxide							
n	9	10	9	9	9	10	10	10
SiO_2	52.9 ± 0.6	52.9 ± 0.6	52.3 ± 0.5	52.4 ± 0.5	52.5 ± 0.6	52.8 ± 0.6	53.2 ± 0.7	53.4 ± 0.4
TiO_2	0.55 ± 0.08	0.50 ± 0.07	0.50 ± 0.10	0.48 ± 0.08	0.51 ± 0.06	0.50 ± 0.07	0.51 ± 0.05	0.49 ± 0.07
Al_2O_3	18.1 ± 0.2	17.9 ± 0.3	17.9 ± 0.4	17.6 ± 0.2	17.9 ± 0.3	18.1 ± 0.2	17.3 ± 0.4	17.7 ± 0.3
FeO_{total}	0.34 ± 0.14	0.33 ± 0.13	1.12 ± 0.23	1.20 ± 0.21	1.15 ± 0.27	0.51 ± 0.19	0.75 ± 0.28	0.17 ± 0.11
MgO	11.5 ± 0.3	11.9 ± 0.3	11.3 ± 0.2	11.5 ± 0.3	11.7 ± 0.2	11.7 ± 0.2	11.9 ± 0.2	12.1 ± 0.3
CaO	13.0 ± 0.2	13.1 ± 0.4	13.1 ± 0.2	13.0 ± 0.2	13.0 ± 0.2	13.0 ± 0.2	12.8 ± 0.4	13.2 ± 0.4
Na_2O	1.49 ± 0.14	1.44 ± 0.16	1.82 ± 0.16	1.74 ± 0.18	1.73 ± 0.15	1.57 ± 0.11	1.71 ± 0.19	1.41 ± 0.13
K_2O	0.77 ± 0.10	0.74 ± 0.08	0.77 ± 0.09	0.76 ± 0.09	0.72 ± 0.07	0.72 ± 0.13	0.76 ± 0.08	0.66 ± 0.08
Total	98.9 ± 0.9	99.0 ± 1.2	99.0 ± 0.8	99.0 ± 0.9	99.3 ± 1.0	99.1 ± 0.5	99.2 ± 1.2	99.3 ± 0.7
$X_{Fe_2O_3}/X_{FeO}$[b]	0.022 ± 0.000	0.031 ± 0.001	0.040 ± 0.001	0.051 ± 0.001	0.050 ± 0.001	0.038 ± 0.001	0.032 ± 0.001	0.023 ± 0.000
$X_{Fe_2O_3}$[b]	0.000 ± 0.000	0.000 ± 0.000	0.000 ± 0.000	0.000 ± 0.000	0.000 ± 0.000	0.000 ± 0.000	0.000 ± 0.000	0.000 ± 0.000
X_{FeO}[b]	0.003 ± 0.001	0.003 ± 0.001	0.009 ± 0.002	0.010 ± 0.002	0.009 ± 0.002	0.004 ± 0.002	0.006 ± 0.002	0.001 ± 0.001
NBO/T	0.61 ± 0.01	0.63 ± 0.02	0.65 ± 0.01	0.65 ± 0.02	0.65 ± 0.02	0.63 ± 0.02	0.66 ± 0.02	0.64 ± 0.02
$Pd_{measured}$ (ppm)	0.97 ± 0.22	1.33 ± 0.31	1.43 ± 0.14	2.05 ± 0.19	2.37 ± 0.19	1.55 ± 0.08	1.23 ± 0.14	1.02 ± 0.14
$Pd_{corrected}$ (ppm)[c]	1.15 ± 0.26	1.47 ± 0.34	1.67 ± 0.16	2.27 ± 0.21	2.59 ± 0.22	1.74 ± 0.10	1.45 ± 0.17	1.14 ± 0.16
Metal:	wt.%							
n	19	18	10	8	6	10	11	14
Fe	6.58 ± 0.67	4.24 ± 0.59	5.95 ± 0.36	4.28 ± 0.42	3.80 ± 1.06	4.67 ± 0.54	6.36 ± 0.46	4.59 ± 0.37
Pd	93.0 ± 0.9	96.0 ± 1.3	93.5 ± 1.0	95.9 ± 1.0	95.8 ± 1.1	95.1 ± 1.0	93.6 ± 1.6	95.5 ± 1.0
Total	99.6 ± 0.8	100.2 ± 1.0	99.5 ± 1.1	100.2 ± 0.9	99.6 ± 0.8	99.8 ± 1.1	100.0 ± 1.6	100.1 ± 1.0
a_{Pd}^{alloy}[d]	0.84 ± 0.02	0.90 ± 0.02	0.86 ± 0.01	0.90 ± 0.01	0.91 ± 0.02	0.89 ± 0.02	0.85 ± 0.02	0.89 ± 0.01
$2\log(X_{FeO}^{silicate}/X_{Fe}^{metal})$	-3.24 ± 0.36	-2.91 ± 0.36	-2.14 ± 0.19	-1.81 ± 0.17	-1.76 ± 0.32	-2.63 ± 0.33	-2.53 ± 0.33	-3.54 ± 0.58

n=number of analyses

[a]reversed experiments; [b]calculated according to the formalism given by Killinc et al. (1983); [c]measured Pd concentrations corrected to unit Pd activity in the metal phase;

[d]calculated from the activity-composition relations given by Tomiska et al. (1989)

All quoted uncertainties are 2σ standard deviation

Table 2.1: continued

sample	PD9	PD10	PD11	PD12	PD13	PD14	PD20	PD23
$\Delta \log pO_2^{FMQ}$	0.5	0	0.5	1	1.5	0	−0.5	6.6
$CO/CO_2/O_2$ (sccm)	10/160/0	10/160/0	10/300/0	8/400/0	5/500/0	20/320/0	27/140/0	air
Glass:	wt.% oxide							
n	12	10	9	9	10	10	10	10
SiO_2	51.4 ± 0.5	52.4 ± 0.5	51.7 ± 0.5	50.4 ± 0.6	48.7 ± 0.7	52.3 ± 0.4	52.5 ± 0.6	48.6 ± 0.6
TiO_2	0.51 ± 0.07	0.48 ± 0.07	0.48 ± 0.06	0.46 ± 0.11	0.46 ± 0.10	0.29 ± 0.08	0.26 ± 0.10	0.26 ± 0.07
Al_2O_3	17.0 ± 0.2	17.4 ± 0.4	17.2 ± 0.4	16.7 ± 0.5	16.1 ± 0.4	17.5 ± 0.4	17.4 ± 0.9	15.9 ± 0.4
FeO_{total}	3.59 ± 0.25	2.31 ± 0.24	3.52 ± 0.17	5.41 ± 0.36	6.89 ± 0.40	1.51 ± 0.31	1.02 ± 0.20	7.64 ± 0.62
MgO	11.6 ± 0.2	11.8 ± 0.2	12.0 ± 0.3	11.9 ± 0.2	11.3 ± 0.1	12.7 ± 0.3	12.6 ± 0.3	12.6 ± 0.4
CaO	12.5 ± 0.4	12.7 ± 0.2	12.6 ± 0.5	12.4 ± 0.3	12.1 ± 0.4	12.9 ± 0.3	13.0 ± 0.2	11.5 ± 0.5
Na_2O	1.86 ± 0.17	1.76 ± 0.15	1.81 ± 0.19	1.79 ± 0.17	2.00 ± 0.18	1.72 ± 0.17	1.70 ± 0.14	1.95 ± 0.14
K_2O	0.73 ± 0.07	0.73 ± 0.05	0.70 ± 0.08	0.64 ± 0.09	0.74 ± 0.11	0.66 ± 0.08	0.74 ± 0.09	0.63 ± 0.05
Total	99.5 ± 0.9	99.7 ± 0.7	100.2 ± 1.2	99.9 ± 0.8	98.5 ± 1.3	99.7 ± 0.8	99.4 ± 1.5	99.2 ± 1.2
$X_{Fe_2O_3}/X_{FeO}$ [b]	0.086 ± 0.002	0.065 ± 0.001	0.085 ± 0.001	0.112 ± 0.002	0.152 ± 0.003	0.064 ± 0.001	0.039 ± 0.001	1.914 ± 0.038
$X_{Fe_2O_3}$ [b]	0.002 ± 0.000	0.001 ± 0.000	0.002 ± 0.000	0.005 ± 0.000	0.008 ± 0.000	0.001 ± 0.000	0.000 ± 0.000	0.043 ± 0.003
X_{FeO} [b]	0.028 ± 0.002	0.018 ± 0.002	0.027 ± 0.001	0.041 ± 0.003	0.052 ± 0.003	0.013 ± 0.002	0.008 ± 0.002	0.022 ± 0.001
NBO/T	0.71 ± 0.01	0.68 ± 0.01	0.72 ± 0.01	0.76 ± 0.01	0.78 ± 0.02	0.71 ± 0.02	0.70 ± 0.03	0.59 ± 0.02
$Pd_{measured}$ (ppm)	6.21 ± 0.52	2.53 ± 0.25	6.39 ± 0.31	13.2 ± 1.5	19.2 ± 2.8	2.96 ± 0.15	1.88 ± 0.15	307 ± 19
$Pd_{corrected}$ (ppm)[c]	6.66 ± 0.57	2.83 ± 0.28	6.85 ± 0.34	13.7 ± 1.6	19.5 ± 2.9	3.26 ± 0.20	2.10 ± 0.19	307 ± 20
Metal:	wt.%							
n	13	10	11	14	14	13	9	7
Fe	3.11 ± 0.23	4.65 ± 0.48	3.11 ± 0.22	1.90 ± 0.21	0.71 ± 0.17	4.08 ± 0.54	4.56 ± 1.28	0.04 ± 0.03
Pd	96.8 ± 1.3	95.1 ± 0.7	97.3 ± 0.7	98.3 ± 0.9	99.5 ± 0.9	95.9 ± 1.8	95.6 ± 2.1	99.4 ± 1.2
Total	99.9 ± 1.2	99.8 ± 0.9	100.4 ± 0.7	100.2 ± 0.9	100.2 ± 0.9	100.0 ± 1.7	100.2 ± 1.4	99.5 ± 1.2
$a_{Pd}^{alloy\,d}$	0.93 ± 0.02	0.89 ± 0.01	0.93 ± 0.01	0.96 ± 0.01	0.99 ± 0.01	0.91 ± 0.03	0.90 ± 0.04	1.00 ± 0.02
$2\log(X_{FeO}^{silicate}/X_{Fe}^{metal})$	-0.62 ± 0.08	-1.33 ± 0.13	-0.64 ± 0.08	0.13 ± 0.11	1.17 ± 0.22	-1.53 ± 0.20	-2.01 ± 0.29	3.00 ± 0.83

n=number of analyses

[a]reversed experiments; [b]calculated according to the formalism given by Killinc et al. (1983); [c]measured Pd concentrations corrected to unit Pd activity in the metal phase;

[d]calculated from the activity-composition relations given by Tomiska et al. (1989)

All quoted uncertainties are 2σ standard deviation

Table 2.1: continued

sample	PD24	PD25	PD30[a]	PD32	PD33	PD35	PD36	PD37
$\Delta \log pO_2^{FMQ}$	4	5	0.5	0.5	0.5	0.5	0.5	0.5
$CO/CO_2/O_2$ (sccm)	15/400/4	15/400/7	10/300/0	10/300/0	10/300/0	10/300/0	10/300/0	10/300/0
Glass:	wt.% oxide							
n	10	10	10	10	10	9	10	10
SiO_2	48.4 ± 0.8	48.7 ± 0.7	51.9 ± 0.4	48.7 ± 0.4	47.0 ± 0.6	40.2 ± 0.3	37.5 ± 0.3	43.3 ± 0.5
TiO_2	0.24 ± 0.06	0.23 ± 0.06	0.47 ± 0.09	0.43 ± 0.09	0.4 ± 0.1	0.35 ± 0.08	0.35 ± 0.09	0.38 ± 0.05
Al_2O_3	16.1 ± 0.3	16.1 ± 0.3	17.0 ± 0.3	16.0 ± 0.2	15.4 ± 0.2	13.1 ± 0.2	11.6 ± 0.1	14.1 ± 0.2
FeO_{total}	7.43 ± 0.25	7.43 ± 0.52	3.04 ± 0.22	8.87 ± 0.43	11.8 ± 0.3	25.05 ± 0.54	30.70 ± 0.81	19.21 ± 0.74
MgO	12.7 ± 0.3	12.6 ± 0.3	12.4 ± 0.2	11.7 ± 0.2	11.2 ± 0.2	9.6 ± 0.2	9.0 ± 0.2	10.2 ± 0.2
CaO	11.7 ± 0.2	11.8 ± 0.2	12.4 ± 0.1	11.6 ± 0.1	11.2 ± 0.2	9.6 ± 0.1	9.0 ± 0.1	10.3 ± 0.1
Na_2O	2.06 ± 0.28	2.05 ± 0.09	1.88 ± 0.13	1.62 ± 0.13	1.6 ± 0.2	0.86 ± 0.11	0.54 ± 0.09	1.12 ± 0.13
K_2O	0.70 ± 0.06	0.73 ± 0.11	0.78 ± 0.04	0.69 ± 0.06	0.7 ± 0.0	0.37 ± 0.04	0.22 ± 0.05	0.49 ± 0.04
Total	99.5 ± 1.1	99.7 ± 0.8	99.9 ± 0.7	99.6 ± 1.0	99.3 ± 0.8	99.2 ± 0.9	98.9 ± 1.3	99.2 ± 1.2
$X_{Fe_2O_3}/X_{FeO}$[b]	0.526 ± 0.016	0.872 ± 0.009	0.085 ± 0.001	0.089 ± 0.001	0.092 ± 0.001	0.099 ± 0.001	0.103 ± 0.001	0.095 ± 0.002
$X_{Fe_2O_3}$[b]	0.022 ± 0.001	0.029 ± 0.002	0.002 ± 0.000	0.006 ± 0.000	0.009 ± 0.000	0.020 ± 0.000	0.026 ± 0.001	0.015 ± 0.001
X_{FeO}[b]	0.041 ± 0.001	0.034 ± 0.002	0.024 ± 0.002	0.069 ± 0.003	0.093 ± 0.002	0.201 ± 0.003	0.247 ± 0.004	0.153 ± 0.004
NBO/T	0.74 ± 0.02	0.68 ± 0.01	0.73 ± 0.02	0.84 ± 0.02	0.90 ± 0.02	1.18 ± 0.01	1.35 ± 0.02	1.04 ± 0.03
$Pd_{measured}$ (ppm)	70.1 ± 7.7	114 ± 3	5.70 ± 0.25	5.54 ± 0.72	5.50 ± 0.55	7.11 ± 0.26	7.37 ± 0.50	5.84 ± 0.56
$P_{dcorrected}$ (ppm)[c]	70.3 ± 7.9	114 ± 5	6.30 ± 0.32	6.62 ± 0.87	6.74 ± 0.69	9.19 ± 0.36	9.67 ± 0.68	7.42 ± 0.73
Metal:	wt.%							
n	7	2	10	9	6	6	9	9
Fe	0.14 ± 0.06	0.04 ± 0.03	4.22 ± 0.24	6.75 ± 0.37	7.54 ± 0.39	9.14 ± 0.21	9.56 ± 0.34	8.55 ± 0.39
Pd	99.3 ± 1.5	99.9 ± 2.1	96.4 ± 1.9	92.4 ± 1.2	91.8 ± 1.3	90.8 ± 0.9	90.2 ± 1.0	90.4 ± 1.7
Total	99.4 ± 1.6	99.9 ± 2.1	100.6 ± 2.0	99.1 ± 1.3	99.3 ± 1.1	100.0 ± 1.1	99.8 ± 1.1	99.0 ± 1.8
$a_{Pd}^{alloy\,d}2$	1.00 ± 0.02	1.00 ± 0.03	0.90 ± 0.02	0.84 ± 0.02	0.82 ± 0.02	0.77 ± 0.01	0.76 ± 0.01	0.79 ± 0.02
$2\log(X_{FeO}^{silicate}/X_{Fe}^{metal})$	2.39 ± 0.36	3.38 ± 0.73	-1.03 ± 0.08	-0.49 ± 0.06	-0.33 ± 0.05	0.19 ± 0.03	0.34 ± 0.03	0.00 ± 0.05

n=number of analyses
[a]reversed experiments; [b]calculated according to the formalism given by Killinc et al. (1983); [c]measured Pd concentrations corrected to unit Pd activity in the metal phase;
[d]calculated from the activity-composition relations given by Tomiska et al. (1989)
All quoted uncertainties are 2σ standard deviation

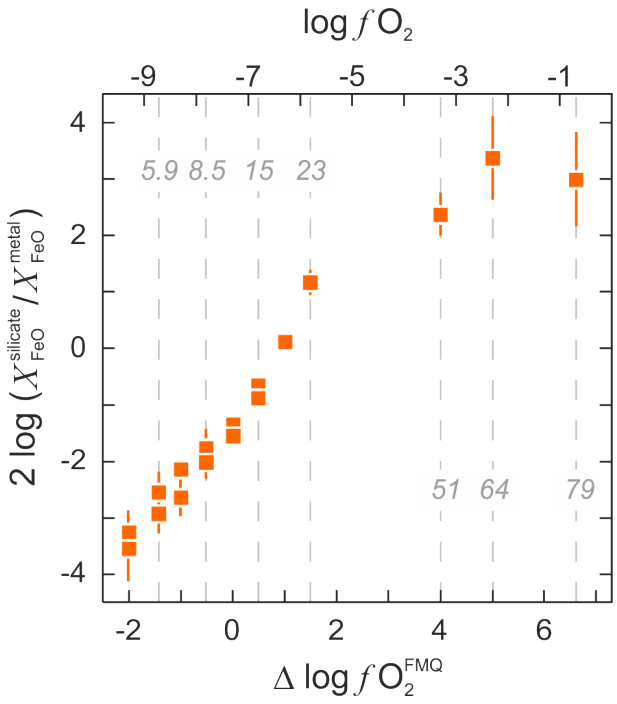

Figure 2.3: Redox exchange of Fe in metal and FeO in the silicate melt versus relative fO_2 (see text). Vertical dashed lines are $(Fe^{3+}/\Sigma Fe)\times 100$ isopleths calculated with the formalism of Kilinc et al. (1983). Note the gradual change in slope around FMQ. Above FMQ+4, Fe in metal phase is smaller than 0.05 wt.% and variations in $2\log(X^{silicate}_{FeO}/X^{metal}_{Fe})$ are within the 2σ errors.

2.4.2 Metal-silicate melt equilibria with palladium

Palladium concentrations in the glass analyzed by LA-ICP-MS are shown in Fig. 2.4 A. For comparison we also show the Pd solubilities in AnDi eutectic melt (Borisov et al., 1994; Fig. 2.4 B). As predicted by Eq. (2.1) and demonstrated by Borisov et al. (1994), Pd concentrations increase with increasing relative fO_2, in the picrite from 1.07 ± 0.26 ppm (FMQ−2) to 306 ± 19 ppm (FMQ+6.6). All concentrations reported here are corrected to unit activity of Pd in the metal phase. Activity coefficients for Pd in the metal phase were calculated by fitting the molar excess Gibbs energies (ΔG^{excess}) obtained at 1292 °C by Tomiska (1989) to the formalism of asymmetric solid solution (Thompson, 1967).

$$\Delta G^{excess} = X_{Pd} \cdot X_{Fe} \cdot (W^G_{Pd} \cdot X_{Fe} + W^G_{Fe} \cdot X_{Pd}) \quad (2.5)$$

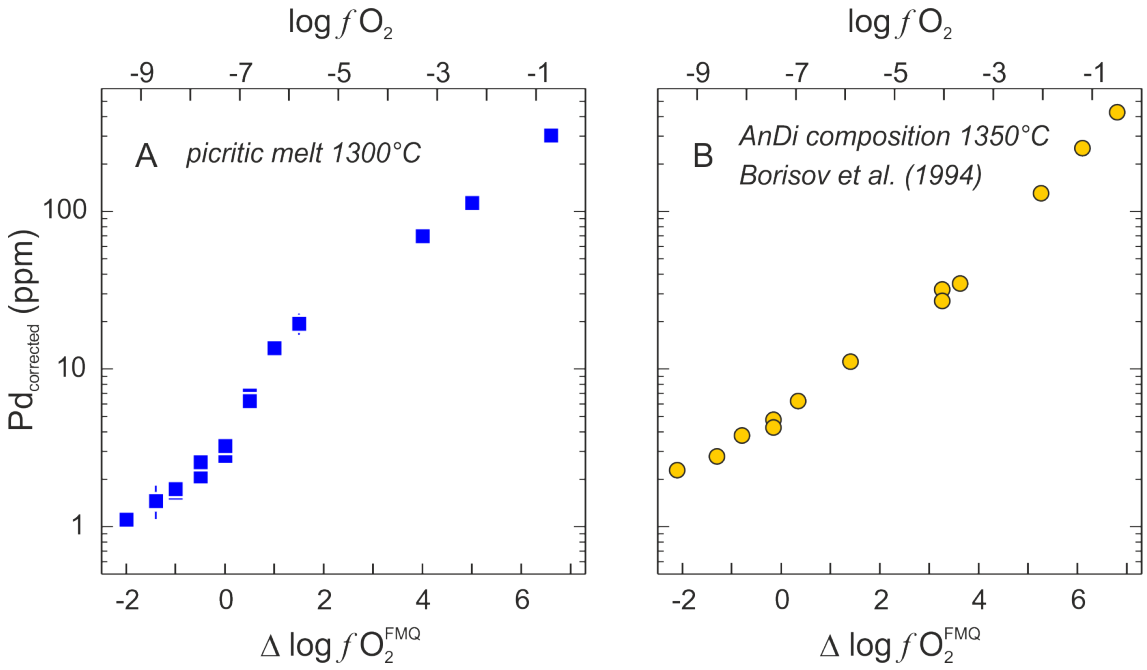

Figure 2.4: (A) Variations in Pd^{n+} concentration in picrite versus relative fO_2; all concentrations corrected to unit Pd activity in the metal phase (cf. Eq. 2.6). Note the change in slope at the same relative fO_2 as in Fig. 2.3 (see Eq. 2.7 and text). Error bars are 2σ, however, most errors are smaller than symbol size. Multiple data points at constant fO_2 represent reversed and/or duplicated experiments (cf. Table 2.1). (B) Palladium solubilities in iron-free AnDi melt at 1350 °C as reported by Borisov et al. (1994) are shown for comparison (reported 1σ uncertainties are 10 % below 10 ppm Pd, and 5 % above 10 ppm Pd).

The Margules interaction parameters obtained with this procedure are $W^G_{\mathrm{Pd}} = -14700\,\mathrm{J/mol}$ and $W^G_{\mathrm{Fe}} = -30450\,\mathrm{J/mol}$, respectively. The activity coefficients for Fe and Pd can then be derived from

$$\mathrm{RT}\ln\gamma_{\mathrm{Pd}} = X^2_{\mathrm{Fe}} \cdot \left[-W^G_{\mathrm{Pd}} + 2 \cdot \left(-W^G_{\mathrm{Fe}} + W^G_{\mathrm{Pd}}\right)\right] \tag{2.6}$$

Between FMQ−2 and FMQ (Fig. 2.4 A), Pd concentrations define a slope in log(concentration) – log(fO_2) space of $\sim 0.22 \pm 0.03$ (2σ) which according to theory (i.e. Eq. 2.3) would be consistent with Pd being present predominantly as a monovalent cation (i.e., Pd^{1+} or formal Pd_2O species). Borisov et al. (1994), in contrast, found in that low fO_2 segment a shallower slope of only 0.17 ± 0.01. These authors hypothesized that below FMQ, neutral species (Pd^0) may become important in conjunction with Pd^{1+}. Interestingly, in that fO_2 range the concentrations measured by Borisov et al. (1994) are also higher than ours by a factor of two. We suspect, therefore, that the alleged neutral (Pd) species is an artifact, i.e. a Pd com-

ponent present as metallic nano-nuggets or even clusters (Tredoux et al., 1995) that is indistinguishable from Pd^{n+} in solution if charges are analyzed by INAA.

Above FMQ, the slope of the solubility profile steepens to $\sim 0.56 \pm 0.10$ (Fig. 2.4 A). From FMQ to ~FMQ+2, the dominant Pd oxidation state appears to be Pd^{2+} and the dominant oxide species PdO. Note that the change in oxidation state occurs within the same relative fO_2 range where $2\log(X_{FeO}^{silicate}/X_{Fe}^{metal})$increases (cf. Fig. 2.3). We suggest that around FMQ, redox exchange equilibria with major metal oxides such as

$$Pd_2O^{silicate} + 2FeO_{1.5}^{silicate} \Leftrightarrow 2PdO^{silicate} + 2FeO^{silicate} \quad (2.7)$$

gain increasing importance, explaining why the change in Pd^{n+} slope coincides so closely with that of $2\log(X_{FeO}^{silicate}/X_{Fe}^{metal})$. Evidently, the effect of iron on Pd (and possibly HSE) solubility in silicate goes well beyond the activity effect on the metal phase identified by Borisov and Palme (2000). Consequently, above FMQ+0.5, our Pd concentrations in picritic melt are well above those reported by Borisov et al. (1994) in AnDi melts.

With further oxidation up to FMQ+6.6, Pd concentrations increase further but not at the same rate as in the lower fO_2 segment between FMQ and FMQ+2 (Fig. 2.4). The same is observed with respect to iron partitioning between metal and silicate (Fig. 2.3). We are hesitant, however, to derive an oxidation state of the dominant Pd cationic species in solution based on that slope (i.e., 0.26 ± 0.04) because this would imply a reduction back to Pd^{1+} even though relative fO_2 increases. Rather, we suspect that at high fO_2 the assumption of ideal behaviour of Pd in silicate melt, implicit in Eq. (2.1), may no longer be valid, and that we see the activity of Pd^{n+} increasing at a rate faster than Pd^{n+} solubility. Mysen et al. (1982) showed that Fe^{3+} tends to polymerize silicate melts, and Hillgren et al. (1996) demonstrated experimentally that solubilities of transition metals tend to decrease when silicate melts polymerize. Hence, for the highly oxidized segment in Fig. 2.4 we refrain from estimating an oxidation state of Pd^{n+} in the silicate melt, but instead attribute the change in slope to changing activity-composition relations imposed by polymerization.

To verify if Eq. (2.7) is valid, several more experiments were performed at constant temperature and fO_2 (1300 °C and FMQ+0.5) with variable FeO. The silicate matrix again was the picritic basalt, this time doped with extra FeO from 3 to 25 wt.%. In the corresponding $X_{FeO-total}$ range from 0.03 to 0.17, iron oxide has little measurable

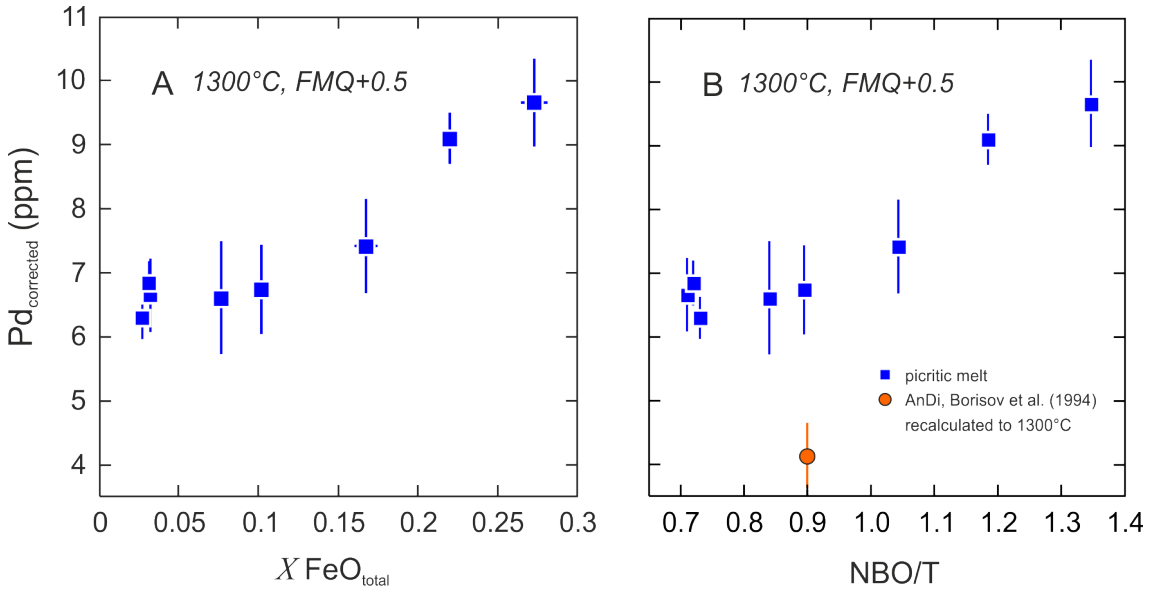

Figure 2.5: (A) Pd concentrations at FMQ+0.5 and 1300 °C versus $X_{\mathrm{FeO-total}}$ (as measured by EPMA; i.e. $X_{\mathrm{FeO}} + X_{\mathrm{Fe_2O_3}}$) in picrite. All concentrations are corrected to unit activity of Pd in the metal phase. (B) Pd concentrations of the same set of experiments versus NBO/T (Mysen et al., 1982). The corresponding Pd concentration in AnDi (1300 °C and FMQ+0.5) was calculated according to the equation describing Pd solubility given by Borisov et al. (1994). 2σ errors in calculated NBO/T are smaller than symbol sizes.

effect on Pd (Fig. 2.5A), but above $X_{\mathrm{FeO-total}} = 0.17$ we note an increase by a factor of two. This could be taken to corroborate our notion expressed by Eq. (2.7) that Pd^{n+} solubility is influenced by electron exchange with FeO and $\mathrm{FeO_{1.5}}$. Unfortunately though, the addition of FeO also lowers the polymerization degree of the silicate melt here expressed as NBO/T (i.e. non-bridging oxygens per tetrahedron; Mysen et al., 1982) from 0.7 to 1.3 (Fig. 2.5 B). Therefore some uncertainty remains as to the relative importance of the fO_2 or NBO/T contributions to Pd solubility. The crucial observation might be that Pd in FeO-free AnDi melt (NBO/T = 0.9) recalculated to 1300 °C, is lower by a factor of $\sim$1.5 than in the corresponding picrite composition with $X_{\mathrm{FeO-total}} = 0.1$, suggesting that the FeO factor on Pd solubility may prevail over NBO/T.

2.5 Discussion and conclusions

The results of this study suggest that FeO und $\mathrm{FeO_{1.5}}$ in silicate melts strongly influence Pd oxidation state and solubility, beyond the effect of Fe in the metal phase. In absolute terms the Pd differences between our data and the AnDi solubilities are

small. However, there is a lot more detail in the picrite solubility profiles than in the AnDi solubilities, also thanks to LA-ICP-MS as tool for spatially-resolved analysis.

From the Pd solubility profile in picritic melt (cf. Fig. 2.4 A) three distinct fO_2 regions can be identified:

- Under moderately reduced conditions up to ∼FMQ, addition of FeO seems to suppress Pd solubility (Fig 2.4 A and B). Presumably this is an artifact: We suggest that the presence of FeO (plus its equilibrium activity of $FeO_{1.5}$) in silicate suppresses the formation of metallic Pd nano-nuggets, implying that the Pd concentrations in AnDi at low fO_2 (cf. Fig. 2.4B) are no real solubilities but caused by metallic Pd nano-nuggets. If indeed neutral HSE species existed in reduced silicate melts (Borisov et al., 1994, Cottrell and Walker, 2006), which is a minority view, then the presence of FeO (plus some $FeO_{1.5}$) would tend to destabilize these species relative to Pd cations (e.g. Brenan et al., 2003; Fortenfant et al., 2006; Ertel et al., 2006, 2008; Medard et al., 2010; Yokoyama et al., 2009).

- In the intermediate fO_2 from FMQ to FMQ+2 where most natural basalts come to lie, our solubilities in FeO-bearing melt are higher than in AnDi. In this fO_2 segment, we also note a marked increase in the slope of $2\log\left(X_{\mathrm{FeO}}^{\mathrm{silicate}}/X_{\mathrm{Fe}}^{\mathrm{metal}}\right)$ vs. fO_2 (Fig. 2.3). A mechanism proposed is that in this fO_2 range redox exchange equilibria such as Eq. (2.7) take effect. In $FeO_{1.5}$ bearing silicate melts, such electron exchange equilibria stabilize a higher oxidation state of the Pd cationic species in the silicate melt relative to iron-free AnDi, because the $FeO_{1.5}$ species is far more abundant than any Pd oxide species. The net effect of FeO-$FeO_{1.5}$ addition in this fO_2 range is to increase Pd solubility (cf. Eq. 2.1).

- In the high fO_2 region above FMQ+2, Pd solubilities are lower compared to the expected Pd as extrapolated from the intermediate fO_2 region. Our favored explanation is that high $FeO_{1.5}$ activities in this fO_2 range increasingly polymerize the silicate melt, introducing marked deviations from ideal solubility and causing Pd^{n+} activities to increase with increasing fO_2 at a rate faster than Pd^{n+} concentrations.

All these effects underline how important it is to supplement experiments in simple

chemical systems with experimentation in compositionally more complex systems, for in AnDi alone none of these effects would have been evident.

The addition of FeO contributes toward an improved understanding in Pd solubility mechanisms in silicate melt. One should stress though that our Pd solubility data do not allow fundamentally new petrologic insights that could not have been gained as well with the AnDi dataset. No matter if we take the AnDi or the picrite Pd solubilities as our reference: all primitive melts derived from the Earth's mantle are Pd-undersaturated. Basalts in the relative fO_2 range from FMQ−1 (MORB) to FMQ+2 (IAB) typical have Pd contents around 20 ppb (e.g. Peach et al., 1990; Woodhead et al., 2002; Bezos et al., 2005). The solubility of Pd in equilibrium with metallic Pd or (Pd,Fe) alloy in that fO_2 range is around two orders of magnitude higher. It does not come as a surprise that neither basalts nor samples from Earth's mantle were ever reported to contain Pd-rich metallic alloys. The high solubility of Pd^{n+} in basaltic melt does not permit the crystallization of such phases from a melt, nor does it allow their survival during partial silicate melting in the mantle.

3 Solubility of Ru and Pd in picritic melt: The effect of sulfur

3.1 Introduction

Various experimental studies (e.g. Borisov and Palme, 2000; Ertel et al., 1999, 2001, 2008; O'Neill et al., 1995) investigated solubilities of the highly siderophile elements (HSE – Os, Ir, Ru, Pt, Pd, Rh, Re and Au) in silicate melts. These studies have shown that HSE solubilities in silicate melt increase with oxygen fugacity (fO_2). The conclusion from these studies was that the HSE dissolve to a large extent as oxides, and are thus associated with O^{2-} as a ligand.

The majority of these experimental studies were carried out in synthetic CaO-MgO-Al_2O_3-SiO_2 (CMAS) melt compositions. However, it becomes increasingly evident that the CMAS melt compositions may not be appropriate for such studies, because melt composition may have a strong influence on the solubility of trace elements in silicate melts (e.g. Borisov and Danyushevsky, 2011; Hillgren et al., 1996; Laurenz et al., 2010; O'Neill and Eggins, 2002; Rose-Weston et al., 2009). In addition, for multivalent elements the amount of Fe dissolved in the silicate is an important parameter. By investigating the solubility of Pd in an FeO-bearing silicate melt, Laurenz et al. (2010) could show that Fe oxide species work to increase Pd solubility compared to its solubility in AnDi melt through a redox exchange.

A parameter that has not been considered systematically is the influence of S on HSE solubility, although the HSE are known to be chalcophile (e.g. Andrews and Brenan, 2002a; Ballhaus et al., 2006; Bezmen et al., 1994; Brenan, 2008; Fleet et al., 1996; Fonseca et al., 2007, 2009, 2011; Peach et al., 1994; Pruseth and Palme, 2004; Stone et al., 1996). In the literature the influence of sulfur on HSE solubility in silicate melts was regarded to be negligible due to thermochemical reasons (e.g. O'Neill et al., 1995; Tuff and O'Neill, 2010). It was argued that the effect of S^{2-} on the activity of $MO_{x/2}^{silicate}$ is negligible, since the concentration of oxygen in silicate melts (~ 45 wt.%) is orders of magnitude higher than sulfur (~ 1000 ppm). However, O'Neill et al. (1995) did not take into account that not all oxygen is available for redox exchange with the atmosphere, i.e. that it might not be appropriate to judge

the role of S based on total oxygen/sulfur ratios in a basaltic melt. In addition, the HSE might show a preference to associate with S^{2-} as a ligand in preference to the O^{2-} ligand owing to their chalcophile nature. If this is the case, HSE solubility in a sulfide-undersaturated silicate melt (i.e. where some S^{2-} is dissolved but an immiscible FeS sulfide melt is not yet present) is expected to be higher than in the S-free AnDi melt, because $MS_{x/2}^{silicate}$ -species are dissolved in addition to $MO_{x/2}^{silicate}$. Indeed few studies indicate that S^{2-} or other chalcogenes might act as a ligand to chalcophile elements (Botcharnikov et al., 2010; Brenan, 2008; Evans et al., 2008; Helmy et al., 2007, 2010; Li et al., 2003).

After Laurenz et al. (2010) investigated the effect of iron on the solubility of Pd in picrite melt, the question that we want to address in this study is what effect sulfur might have. We report the results of experiments where Ru or Pd metal are equilibrated with picrite melt under controlled oxygen and sulfur fugacities (fO_2 and fS_2, respectively). Ruthenium and Pd were chosen because they are the most chalcophile of the HSE (e.g. Andrews and Brenan, 2002b; Makovicky et al., 1990). The addition of S to a Pd-metal saturated silicate melt triggers sulfide melt exsolution, because Pd metal is not stable at magmatic temperature at any experimentally accessible fS_2, illustrating the effect of sulfide saturation: Palladium concentrations in the sulfide saturated picrite melt are lower when compared to the S-free system (Laurenz et al., 2010), reflecting the strong partitioning of Pd into the sulfide phase. On the other hand, Ru solubility in our experiments is enhanced by more than one order of magnitude in S-bearing, and sulfide-undersaturated silicate melts relative to S-free compositions at identical fO_2. Ruthenium associates with the S^{2-} ligand and dissolves as RuS_2-species in the silicate melt in addition to the oxide species. Ruthenium and possibly other HSE as well, are then shown to form strong associations with the S^{2-} ligand in a silicate melt in preference to the O^{2-} ligand.

3.2 The solubility of HSE in silicate melts

Previous experimental studies have shown that the HSE are dissolved in S-free silicate melts as oxides species (Borisov and Palme, 1995, 1997, 2000; Capobianco and Hervig, 1996; Capobianco et al., 1993; Cottrell and Walker, 2006; Ertel et al., 1999, 2001, 2006, 2008; Fortenfant et al., 2003, 2006; Laurenz et al., 2010; O'Neill et al., 1995; Yokoyama et al., 2009). According to these studies, the dissolution can be described

by:

$$\mathrm{M^{alloy}} + \frac{\mathrm{x}}{4}\mathrm{O_2} \Leftrightarrow \mathrm{MO^{silicate}_{x/2}} \tag{3.1}$$

where x is the valence state of the metal (M) in the silicate melt. The activity of the HSE oxide species in solution in silicate melt ($a^{\mathrm{silicate}}_{\mathrm{MOx/2}}$) is given by:

$$\log a^{\mathrm{silicate}}_{\mathrm{MO_{x/2}}} = \log K + \log a^{\mathrm{alloy}}_{\mathrm{M}} + \frac{\mathrm{x}}{4}\log fO_2 \tag{3.2}$$

Where K is the equilibrium constant of reaction (3.1). If the metal is pure (i.e. not diluted by Fe), its activity ($a^{\mathrm{alloy}}_{\mathrm{M}}$) is unity. Assuming $\gamma^{\mathrm{silicate}}_{\mathrm{MO_{x/2}}}$ is independent of $f\mathrm{O_2}$, equation (3.2) simplifies to:

$$\log a^{\mathrm{silicate}}_{\mathrm{MO_{x/2}}} = \frac{\mathrm{x}}{4}\log fO_2 + const. \tag{3.3}$$

The valence of the cationic species dissolved in the melt can be derived from the slope ($m = \frac{\mathrm{x}}{4}$) of the solubility curve in $\log X$ – $\log f\mathrm{O_2}$ space.

If the system is S-bearing, the HSE cationic species may also associate with the $\mathrm{S^{2-}}$ ligand provided the melt is sufficiently reduced to be in the sulfide stability field (Jugo et al., 2005, 2010; Mètrich et al., 2009). An exchange equilibrium is thus established between the oxide and sulfide metal species in silicate melt, according to:

$$\mathrm{MO^{silicate}_{x/2}} + \frac{\mathrm{x}}{4}\mathrm{S_2} \Leftrightarrow \mathrm{MS^{silicate}_{x/2}} + \frac{\mathrm{x}}{4}\mathrm{O_2} \tag{3.4}$$

The addition of S shifts this equilibrium (Eq. 3.4) to the left hand side, promoting the formation of an $\mathrm{MS^{silicate}_{x/2}}$ compound, and increasing the solubility of a chalcophile element such as the HSE in the silicate melt relative to the S-free melt.

3.3 Experimental and analytical methods

The solubility experiments were carried out in a one-atm vertical muffle tube furnace equipped for gas mixing. The starting silicate melt composition was a picritic basalt, henceforth called picrite, from the Solomon Islands (SE1 – Rohrbach et al., 2005; Schuth et al., 2004). The picrite powder was placed into an MgO capsule together with Ru-metal powder or Pd-metal foil. Prior to each experiment, the inner walls of the MgO capsules were coated with a mixture of FeO and $\mathrm{SiO_2}$ (1:1) powders and sintered at 1300 ℃ and FMQ−1 for 1.5 hours. This creates a thin melt film along

the MgO grain boundaries, stabilizes the sintered MgO, and generally minimizes the contamination of the picrite melt by MgO. The loop technique conventionally employed for this kind of studies (e.g. Borisov et al. 1994, Laurenz et al., 2010) could not be used, because Ru is only available as metal powder. Furthermore Pd metal proved to be unstable in the fS_2 range accessible by our experiments (see section 4.3 for details). Selected experiments were reversed by doping the picrite starting composition with 0.5 wt.% of either PdO_2 or RuO_2. By doing so, equilibrium was approached from both the oxidized (i.e. initially HSE-rich melt) and the reduced (i.e. initially HSE-free melt) sides. Both forward and reversed charges were equilibrated simultaneously. Hence, they were exposed to identical gas atmospheres. The concentrations of HSE in forward and reversed charges were found to be identical within error (Table 3.1).

The experimental charge was then suspended in the hot zone of the furnace at a temperature of 1300 ± 1 °C. Temperature was controlled with a Type B ($Pt_{94}Rh_6$–$Pt_{70}Rh_{30}$) thermocouple calibrated against the melting point of Au. Oxygen and sulfur fugacities were imposed by CO–CO_2 ($\pm SO_2$) gas mixtures. Fugacities were calculated with an open-source EXCEL® spreadsheet written by Kress et al. (2004), using the thermodynamic data listed in NIST-JANAF tables (Chase, 1998). Calculated fO_2 values were verified regularly using a CaO-Y_2O_3-stabilized ZrO_2 solid electrolyte cell and were found to be accurate to within 0.2 log units of the calculated values.

Unlike the fO_2, the fS_2 cannot be verified independently to be accurate by direct measurement. Nonetheless, fS_2 can be monitored indirectly by using the the molar fraction of FeS in hexagonal pyrrhotite ($Fe_{1-x}S$) synthesized in the gas mixture of interest. Toulmin and Barton (1964) showed that the molar fraction of FeS is a function of fS_2. Unfortunately, that fS_2 sensor only works up to the temperature where hexagonal pyrrhotite is stable (~ 1200 °C), which is 100 °C below our run temperature. However, if fugacities at lower temperature can be shown to be accurate, we can safely assume fS_2 to be correct at our run temperature of 1300 °C.

Table 3.1: Experimental conditions and major elements of the glasses and metal as well as the Ru, S & Pd concentrations. Ru and Pd concentrations were analyzed by LA-ICP-MS.

sample	RU1	RU3	RU5	RU7[a]	RU11[a]	RU12	RU34[a]	RU39	RU40
$\Delta \log fO_2^{FMQ}$	−1	1	−0.5	−1	0	0	−0.5	1	0.5
$\log fS_2$	–	–	-	−2.23	–	–	−2.23	–	–
duration	48	48	48	13	48	48	30	48	48
$CO/CO_2/SO_2$ (sccm)	54/280/0	6/300/0	10/300/0	72/300/30	10/160/0	10/160/0	19/125/38	7.5/375/0	10/325/0
SiO_2	46.2 ± 0.6	48.9 ± 0.7	48.9 ± 0.25	48.5 ± 0.51	47.7 ± 0.55	46.7 ± 0.51	46.9 ± 1.11	47.2 ± 0.59	46.5 ± 0.25
TiO_2	0.73 ± 0.07	0.51 ± 0.11	0.74 ± 0.06	0.19 ± 0.06	0.19 ± 0.09	0.62 ± 0.13	0.28 ± 0.07	0.27 ± 0.08	0.29 ± 0.08
Al_2O_3	12.3 ± 0.2	8.5 ± 0.2	13.6 ± 0.29	11.5 ± 0.20	13.0 ± 0.39	10.2 ± 0.12	10.2 ± 0.21	11.2 ± 0.28	10.9 ± 0.19
FeO	15.4 ± 0.5	17.2 ± 0.7	14.2 ± 0.39	17.6 ± 0.56	14.7 ± 0.90	19.4 ± 0.49	22.9 ± 0.46	20.9 ± 0.75	21.0 ± 0.67
MgO	14.8 ± 0.4	16.7 ± 0.4	14.4 ± 0.27	11.4 ± 0.26	11.3 ± 0.10	14.4 ± 0.32	10.4 ± 0.39	11.5 ± 1.41	11.4 ± 0.24
CaO	8.76 ± 0.27	6.07 ± 0.16	6.42 ± 0.15	8.42 ± 0.18	9.73 ± 0.11	7.07 ± 0.20	7.54 ± 0.39	7.91 ± 1.11	7.98 ± 0.09
Na_2O	1.68 ± 0.16	1.53 ± 0.10	1.69 ± 0.12	1.55 ± 0.16	2.01 ± 0.13	1.43 ± 0.13	1.68 ± 0.25	1.87 ± 0.23	1.77 ± 0.15
K_2O	0.63 ± 0.09	0.50 ± 0.04	0.63 ± 0.09	0.55 ± 0.09	0.66 ± 0.07	0.49 ± 0.06	0.54 ± 0.04	0.63 ± 0.09	0.60 ± 0.03
Total	100.5	99.9	100.6	99.9	99.4	100.3	100.4	101.4	100.4
S (ppm)	n.a.	n.a.	n.a.	650 ± 34	n.a.	n.a.	340 ± 76	n.a.	n.a.
Ru (ppm)	0.05 ± 0.01	0.29 ± 0.08	0.03 ± 0.02	0.16 ± 0.06	0.02 ± 0.01	0.03 ± 0.01	0.64 ± 0.14	0.39 ± 0.18	0.15 ± 0.02
Pd (ppm)	n.a.	n.a.	n.a.	n.a.	n.a.	n.a.	n.a.	n.a.	n.a.

[a] reversed experiments

All quoted uncertainties are 2σ standard deviation

Table 3.1: continued

sample	RU42	RU49[a]	RU54	RU55[a]	RU64	RU65	PD16	PD19	PD22
$\Delta \log fO_2^{FMQ}$	2	0.5	0	0	−1	−0.5	−1	−0.5	0
$\log fS_2$	–	–	−2.26	−2.26	−2.23	−2.23	−2.23	−2.23	−2.23
duration	48	48	48	48	48	48	13	13	13
$CO/CO_2/SO_2$ (sccm)	5/810/0	10/300/0	8/60/67	8/60/67	34/100/10	10/63/19	72/300/30	19/125/38	8/60/67
SiO_2	46.8 ± 0.45	48.8 ± 0.49	48.2 ± 0.38	47.9 ± 0.42	48.5 ± 0.33	48.7 ± 0.40	51.0 ± 0.62	49.3 ± 0.47	48.7 ± 0.7
TiO_2	0.27 ± 0.07	0.38 ± 0.10	0.42 ± 0.10	0.45 ± 0.06	0.45 ± 0.10	0.44 ± 0.07	0.18 ± 0.07	0.19 ± 0.10	0.21 ± 0.07
Al_2O_3	10.8 ± 0.12	14.2 ± 0.15	16.2 ± 0.26	16.7 ± 0.21	16.1 ± 0.19	16.4 ± 0.24	11.0 ± 0.24	12.2 ± 0.22	12.5 ± 0.3
FeO	20.2 ± 0.80	13.3 ± 0.41	9.79 ± 0.12	9.18 ± 0.41	9.60 ± 0.45	9.40 ± 0.32	16.4 ± 0.86	15.9 ± 0.65	15.8 ± 0.7
MgO	11.4 ± 0.26	11.3 ± 0.19	11.6 ± 0.21	11.5 ± 0.21	11.3 ± 0.19	11.4 ± 0.26	11.2 ± 0.27	11.0 ± 0.30	11.5 ± 0.2
CaO	7.74 ± 0.15	10.2 ± 0.15	11.8 ± 0.13	12.3 ± 0.14	11.3 ± 0.23	11.8 ± 0.12	8.05 ± 0.26	8.95 ± 0.20	9.08 ± 0.12
Na_2O	1.73 ± 0.17	1.87 ± 0.15	2.14 ± 0.11	2.29 ± 0.10	2.33 ± 0.21	2.27 ± 0.17	1.70 ± 0.17	1.74 ± 0.17	1.76 ± 0.27
K_2O	0.60 ± 0.03	0.71 ± 0.04	0.74 ± 0.06	0.81 ± 0.04	0.79 ± 0.04	0.78 ± 0.08	0.55 ± 0.10	0.60 ± 0.07	0.61 ± 0.06
Total	99.4	100.7	100.9	101.1	100.4	101.3	100.2	99.9	100.2
S (ppm)	n.a.	n.a.	140 ± 40	130 ± 55	296 ± 36	78 ± 32	299 ± 32	240 ± 62	155 ± 71
Ru (ppm)	3.76 ± 0.68	0.13 ± 0.03	1.00 ± 0.23	1.22 ± 0.31	0.14 ± 0.11	0.59 ± 0.25	n.a.	n.a.	n.a.
Pd (ppm)	n.a.	n.a.	n.a.	n.a.	n.a.	n.a.	0.65 ± 0.14	0.91 ± 0.07	1.3 ± 0.30

[a] reversed experiments

All quoted uncertainties are 2σ standard deviation

To verify the calculated fS_2 values, pyrrhotite was synthesized at 1000 °C in a CO–CO_2–SO_2 (25/0/250) gas mixture. The fS_2 at run conditions was calculated to be 0.032 atm, corresponding to a log fS_2 of −1.5, or ∼5.5 log-units above the Fe-FeS buffer (cf. Scott, 1974). To prevent the formation of Fe oxides, the fO_2 was kept inside the stability field of metallic Fe (FMQ−4 $\widehat{=}$ $IW - 0.3$).
Two starting materials were used to approach the equilibrium from both the reduced and the oxidized sides, i.e. metallic Fe powder and natural pyrite (FeS_2):

$$(2 - 2x)Fe + S_2(gas) = 2Fe_{1-x}S \tag{3.5}$$

$$(1 - x)FeS_2 = Fe_{1-x}S + (0.5 - x)S_2 \tag{3.6}$$

Both starting compositions were placed in individual corundum crucibles, suspended simultaneously in the furnace, and equilibrated with the gas phase for 72 h. Both starting materials yielded homogeneous hexagonal pyrrhotite ($Fe_{1-x}S$) crystals. The pyrrhotite crystals were powdered individually and mixed with a metallic Si standard with a known d-spacing (i.e. NIST SRM 640). Subsequently, the d(102) spacing of pyrrhotite was measured using a Siemens D5000 diffractometer and CuKα radiation. Both pyrrhotite aliquots returned the same d(102) of 2.073 ± 0.001 Å. The Fe content of the $Fe_{1-x}S$ phase calculated from that d-value (Scott, 1974) is 47.9 ± 0.1 at.%. The log fS_2 in equilibrium with this pyrrhotite composition at 1000 °C was then calculated using the formalism given by Toulmin and Barton (1964) to be −1.2 ± 0.2. Considering that Toulmin and Barton (1964) quote an error on their regression of around ± 0.35 log units in fS_2, this value is in excellent agreement with the fS_2 calculated thermodynamically from the gas mixture (i.e. $\log fS_2 = -1.5$).

After a run time of 48 hours experiments were quenched in air to homogeneous glasses by drawing the samples to the water-cooled top of the furnace (∼ 100 °C). Subsequently, the samples were mounted in epoxy resin and polished for microprobe and LA-ICP-MS analysis. Examples of Backscatter Electron (BSE) images of quenched run products are shown in Fig. 3.1.

3.3.1 Electron microprobe analysis

Experimental run products (metal, sulfide and silicate glass) were analyzed for their major element compositions with a JEOL JXA 8900 electron microprobe analyzer (EMPA) in wavelength dispersive mode (WDS) with an accelerating voltage of 15 kV

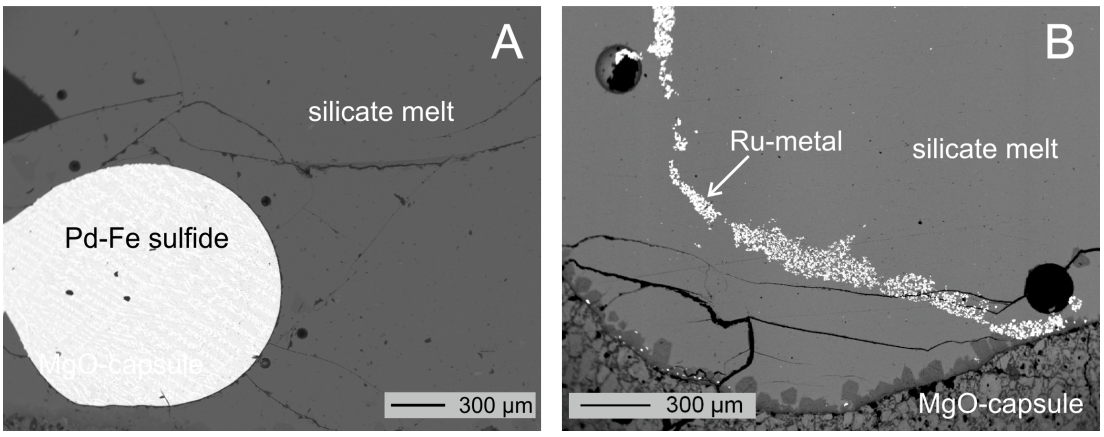

Figure 3.1: Representative Backscatter Electron (BSE) images of quenched experiments (A) Pd-rich sulfide in contact with picrite melt of experiment Pd18. The Pd-metal added to the starting mix completely reacted with the SO_2 of the atmosphere to form Pd-rich sulfide. (B) Ru-metal in contact with the picrite melt. No sulfide phase is present in the experiments addressing Ru-solubility.

and a beam current of 15 nA. Standards used were natural silicates and oxides for glass analysis, and pure Pd, Ru and Fe metal for the metal phases. Sulfides were analyzed using Canyon Diablo troilite (FeS) for the calibration of Fe and S, and pure Pd metal for Pd. Glasses and sulfides were analyzed with a beam defocused to 10 µm and 20 µm, respectively, while the metals were analyzed in spot mode. Counting times were 10 s on peak and 5 s on background, except for Na and K, which were measured with 5 s and 2.5 s respectively in order to avoid alkali migration. Matrix corrections were performed with the ZAF correction method.

The S^{2-} anion is poorly soluble in basaltic melts and difficult to quantify. At FeS saturation typical S^{2-} concentrations in basaltic melts at 1300 °C (our run temperature) are ∼1000 ppm (O'Neill and Mavrogenes, 2002). If FeS saturation is not reached, as in the experiments reported here, S^{2-} concentrations are even lower. Furthermore, the S_{K_α} peak position depends on the valence state of S (Caroll and Rutherford, 1988; Wallace and Carmichael, 1992) and may change during the analysis due to electron beam damage. Therefore, S was analyzed using a peak area routine where two spectrometers (PETH crystals) were scanned across the sulfur K_α peak simultaneously. The total peak area was then integrated to obtain S concentration. Scanning time was set to 300 s, and the probe current to 100 nA, in order to reduce the detection limit for S. The primary standard used to calibrate S was Canyon Diablo troilite (FeS). Secondary glass standards used to cross-check the quality of the calibration were NIST 610 (∼575 ppm S – Jochum et al., 2011) and VG 2

(∼ 1400 ppm S – Jarosewich et al., 1980; O'Neill and Mavrogenes, 2002). The S concentrations determined here were 600 ± 40 ppm for NIST 610 and 1440 ± 30 ppm for the VG 2 glass, which are in good agreement with previously reported values (e.g. Evans et al., 2008; Jochum et al., 2006; O'Neill and Mavrogenes, 2002; Wallace and Carmichael, 1992 and references therein).

3.3.2 Laser-ablation ICP-MS analysis

The HSE in the silicate were analyzed with laser ablation inductively coupled plasma mass spectrometry (LA-ICP-MS). Analyses of the concentrations of Ru in the glasses were carried out using a Q-switched Nd:YAG laser (New Wave Research UP-213; 213 nm wavelength) coupled to a Thermo Finnigan ELEMENT 2 sector field (SF) ICP-MS at the Max-Planck Institut für Chemie in Mainz, Germany. The laser system was operated at a pulse rate of 20 Hz and an energy density of 13 J/cm^2. Spot sizes ranged between 55 and 80 µm depending on concentration levels. Data were collected in time-resolved mode with 12 to 20 s measurement of gas background, followed by 60 s of measurement during laser ablation. Isotopes recorded were ^{25}Mg, ^{29}Si, ^{57}Fe, ^{59}Co, ^{61}Ni, ^{62}Ni, ^{99}Ru, ^{101}Ru and ^{102}Ru. The natural isotope ratios of Ru were well reproduced, showing that there were no significant interferences from other isotopes or molecular compounds. Using ^{57}Fe as an internal standard, Ru concentrations were calibrated against the $(Fe, Ni)_{1-x}S$ in-house reference material synthesized by Wohlgemuth-Ueberwasser et al. (2007). Examples of time-resolved laser spectra are shown in Fig. 3.2. In cases where the spectra showed spikes in the Ru signal (Fig. 3.2 A), presumably due to the presence of metal micro- and nano-nuggets in the silicate glass, only ablation intervals between these spikes were quantified, following the approach of Ertel et al. (2006, 2008).

Palladium concentrations were determined at the Inco Innovation Centre at the Memorial University of New Foundland (Canada), using a GeoLas Pro laser ablation system coupled to a Finnigan Element XR ICP-MS. The analytical details were identical to those reported by Laurenz et al. (2010). To check that the silicate glass is homogeneous, hence verify that equilibrium was reached, up to 15 points were randomly distributed across each polished glass shard. No major compositional inhomogeneities were detected. Forward and reverse experiments were also found to be identical in major element composition and Ru and Pd concentration, so it is assumed that redox equilibrium was generally achieved.

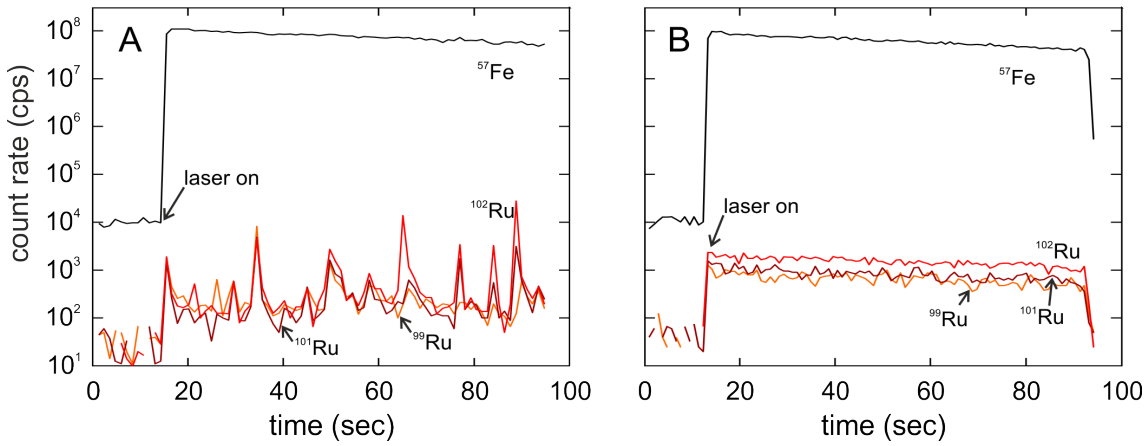

Figure 3.2: Examples of time resolved LA-ICP-MS spectra of two experiments showing ^{57}Fe used as the internal standard and the three measured Ru isotopes (^{99}Ru, ^{101}Ru, ^{102}Ru). (A) Spikes in the time-resolved ablation signal reveal the presence of numerous nanonugget inclusions in the silicate melt in the reduced experiments below FMQ. These spikes were avoided for quantification, however, calculated values are regarded as maximum values. (B) The more oxidized experiments show flat ablation patterns, with only rare spikes in the signal.

3.4 Results

3.4.1 The solubility of Ru and Pd in picrite as a function of fO_2

The concentration of Ru in picrite is shown in Fig. 3.3. Superimposed are the solubilities of Pd in picrite as reported by Laurenz et al. (2010). The measured Pd concentrations in picrite were corrected to unit activity of Pd in the metal phase. Ruthenium concentrations can be taken directly as solubilities, because the metal in these charges is almost pure Ru (<0.4 wt.% Fe). From the activity-composition relationships in the Ru-Fe binary at 1300 °C (Swartzendruber and Sundman, 1983) it follows that the activity of Ru in the metal is close to unity.

As expected from theory and from previous studies (e.g. Borisov et al., 1994; Borisov and Nachtweyh, 1998; O'Neill et al., 1995), Ru as well as Pd solubilities in picrite increase with increasing fO_2. Overall, Ru solubilities in picrite are significantly lower than those reported for Pd (Laurenz et al., 2010). Ruthenium solubility in picrite increases from 0.03 ± 0.01 ppm (FMQ) to 3.7 ± 0.7 ppm (FMQ+2), while Pd solubilities are an order of magnitude higher (Fig. 3.3). Around FMQ, Pd changes its oxidation state from Pd^{1+} to Pd^{2+} (Laurenz et al., 2010). In comparison, the oxidation state of Ru is uniformly Ru^{4+}. The slope in log C_{Ru} - log fO_2 space is 1.06 ± 0.08 (2σ), which is consistent with Ru dissolving as Ru^{4+} cationic species

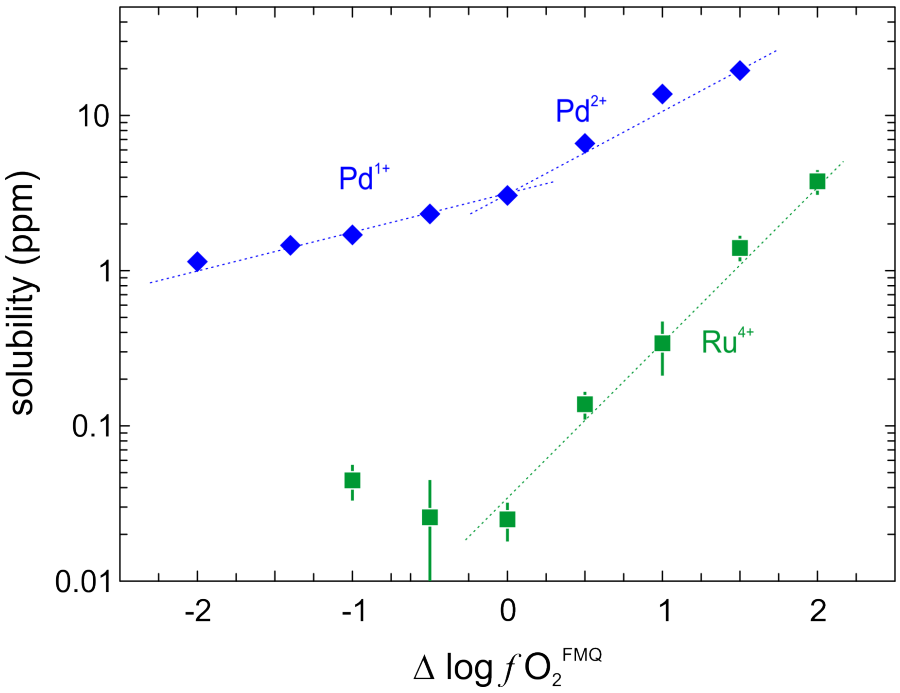

Figure 3.3: Solubilities of Ru and Pd in picrite melt are shown as a function of fO_2. Overall Pd and Ru solubilities increase with fO_2. Palladium shows a transition from Pd^{1+} to Pd^{2+} at around FMQ (Laurenz et al., 2010). Between FMQ and FMQ+2 Ru dissolves as Ru^{4+} in the picrite melt. Regression on the solubility of Ru yields a slope of 1.06 ± 0.08 (2σ) consistent with Ru^{4+}. Below FMQ the concenrations are regarded to be maximum values, because numerous micronuggets can be detected in the LA-ICP-MS spectra (cf. Fig. 3.2 and see text). Solubility values shown are weighted means of individual experiments. Error bars represent 2σ standard deviation.

(Eq. 3.3), reacting with O^{2-} in the melt to form RuO_2. This is in contrast to the observation made by Borisov and Nachtweyh (1998) who found that in synthetic AnDi silicate melt, Ru was dissolving as Ru^{3+} between FMQ±3 and FMQ+5 at 1400 °C. This might be a consequence of whether or not the silicate melt contains FeO.

Below FMQ, Ru is no longer correlated with fO_2. At the same time, the time-resolved laser spectra of these glasses were distinctly spiky (cf. Fig. 3.2 A). Following Ertel et al. (2006, 2008) we attribute these spikes to nano-sized Ru metal inclusions that become more abundant under reducing conditions. Given the complexities of the Ru laser spectra, all concentrations reported for runs below FMQ are considered to be maximum concentrations.

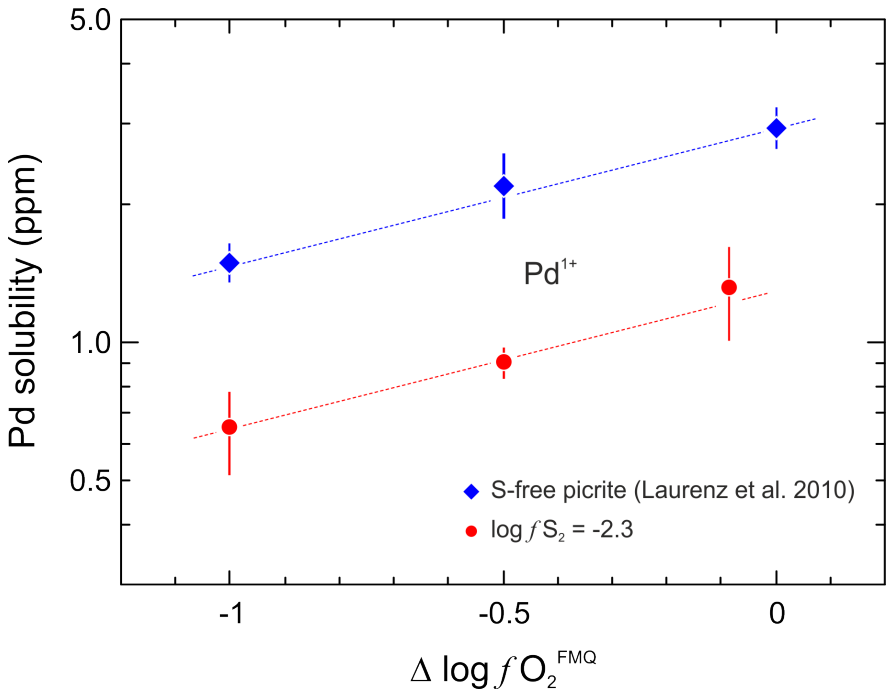

Figure 3.4: Pd concentrations in in S-free (Laurenz et al., 2010) and sulfide saturated picrite melts are shown as a function of fO_2. The Pd concentrations in the sulfide saturated picrite melts of this study are lower by a factor of two compared to the solubilities in picrite determined by Laurenz et al. (2010), as a result of lower Pd activity in the Pd-rich sulfide melt. Solubility values shown are weighted means of individual experiments. Error bars represent 2σ standard deviation.

3.4.2 The effect of sulfur on Ru and Pd solubility in picrite

When S^{2-} is present as an in a silicate melt in addition to O^{2-} the HSE concentrations are expected to increase (cf. section 3.2). For Pd we observe the opposite effect (Fig. 3.4). For Pd the effect of adding S is to lower its concentration in picrite by a factor of two, compared with the Pd solubilities in S^{2-} free melts at the same fO_2 (Laurenz et al., 2010). The reason is, that Pd is unstable as a metal when the gas phase in the furnace contains SO_2. Whenever SO_2 was added to the gas, Pd metal reacted instantly with S^{2-} of the gas and FeO of the silicate, to form a Pd-rich, FeS-bearing, immiscible sulfide melt, with $\sim$80 wt.% Pd, 5 wt.% Fe, and 15 wt.% S. Even at a log fS_2 of -5, the lowest sulfur fugacity we can impose at 1300 °C with our mass flow controllers, Pd metal reacted to form a sulfide melt within minutes. These observations are consistent with results reported by Fonseca et al. (2009), who noted that their sulfide melts remained Pd-undersaturated regardless of the amount of Pd metal they added to their sulfide-bearing experimental charges.

The drop in Pd concentration in the picrite we see in Fig. 3.4 with the addition of S^{2-}, at first counter-intuitive, results because the activity of Pd is lowered when the metal reacts to a $Pd_{1+x}S$ melt. The drop in activity and the resulting drop in the concentration of the Pd cationic species in the picrite is so strong that it completely masks any possible increase in Pd solubility imposed by S. Nevertheless, the slope in $\log C_{Pd}$ – $\log fO_2$ space for the S-bearing experiments remains the same (~ 0.25) as in the S-free experiments reported by Laurenz et al. (2010). This indicates that the presence of S^{2-} in the melt has no major effect on the oxidation state of Pd cationic species (Pd^{1+}) in picrite melts (cf. Eq. 3.3), regardless of the presence of an immiscible sulfide melt.

In contrast to Pd, Ru-metal has a large stability field in sulfur-bearing silicate melts. At 1300 °C, the sulfur fugacity corresponding to the Ru–RuS_2 equilibrium is $\sim \log fS_2 = -1$ bar (Bockrath et al., 2004b). Our runs with Ru-metal and sulfur in silicate were carried out with a sulfur fugacity of $\log fS_2 = -2.3$, and Ru-metal (~ 99.6 wt.% Ru) was stable in all of our experiments (Fig. 3.2 B). Run products do not show any sulfide phase coexisting with the silicate melt. Therefore, any change in Ru-concentration in the picrite with the addition of SO_2 can be attributed solely to the effect of S^{2-} dissolved in the silicate melt.

Indeed, in the S^{2-}-bearing melts Ru solubilites are much higher than in the S-free melts at identical fO_2 (Fig. 3.5). For example, the S-free experiment at FMQ returned a glass with 0.025 ± 0.009 ppm Ru, whereas the equivalent S-bearing experiment ($\log fS_2 = -2.3$ – 140 ppm S) produced a glass with 1.00 ± 0.23 ppm. More oxidizing experiments containing sulfur were not possible, because fO_2 and fS_2 correlate negatively using CO-CO_2-SO_2 gas mixes, so that they can only be varied independently over a limited range. All S-bearing experiments are compared with S-free experiments in Fig. 3.5. In $\log c_{Ru}$ – $\log fO_2$ space, the slope does not change with the addition of S^{2-} (Fig. 3.5). This observation indicates that the oxidation state of the Ru cationic species in silicate melt (i.e. Ru^{4+}) is unaffected by the presence of sulfur.

The effect of sulfur on Ru dissolution in silicate melt can then be expressed as:

$$RuO_2^{silicate} + 2S^{2-} \Leftrightarrow RuS_2^{silicate} + 2O^{2-} \tag{3.7}$$

The addition of S^{2-} to an O^{2-}-bearing silicate is to shift the equilibrium to the right-

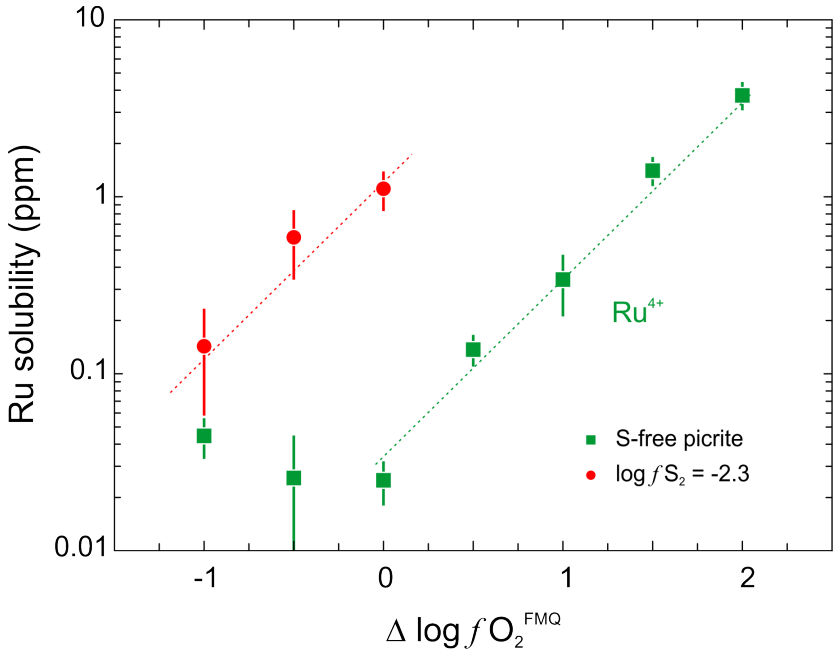

Figure 3.5: Ru solubilities in picrite melt at log $fS_2 = -2.3$ are shown as a function of fO_2. At log $fS_2 = 10^{-2.3}$ Ru solubility is found to be higher by more than one order of magnitude compared to the S-free picrite melt, showing a strong influence of S on Ru solubility. The slopes in both sets of experiments are identical, indicating that the presence of S does not change the oxidation state of Ru. Solubility values shown are weighted means of individual experiments. Error bars represent 2σ standard deviation.

hand side of Eq. 3.7. Because an additional ligand (S^{2-}) is added to the system, an additional species ($RuS_2^{silicate}$) is stabilized in addition to the $RuO_2^{silicate}$ species. Therefore, Ru concentration increases. Note, that order to observe this effect, fS_2 may not exceed a value where FeS becomes a stable phase. Otherwise, Ru metal would become unstable and would be dissolved in the FeS liquid, which is reported to be able to accommodate wt.% levels of Ru (Andrews and Brenan, 2002b). The activity of Ru would decrease, and Ru concentrations in the silicate melt would to decrease accordingly, as is observed for Pd in this study (Fig. 3.4).

3.5 Discussion

The results of our experiments have shown that S^{2-} has a major effect on HSE solubility in silicate melts, much more than previously thought (O'Neill et al., 1995). However, this can only be deduced from the Ru-bearing experiments containing. In the case of Pd there is no fO_2 - fS_2 combination at 1300 °C accessible with our gas flow meters where Pd is stable as a metal phase.

3.5.1 Is sulfur more important as a ligand to HSE than oxygen?

Based on the mass ratio between O^{2-} and S^{2-} in basaltic melts (45 wt.% and $\sim$1000 ppm respectively), it was argued that the effect of S^{2-} on HSE solubility should be negligible when compared to that of the O^{2-} ligand (e.g. O'Neill et al., 1995; Tuff et al., 2010). The results of our experiments are contrary to this notion. We found a marked increase in Ru solubility in picrite (Fig. 3.5). We interpret this observation to indicate a distinct preference of the HSE cationic species to associate with the S^{2-} anionic ligand, over the O^{2-} ligand. O'Neill et al. (1995) considered all oxygen in the melt, including oxygen that is part of the melt structure (i.e. bridging-O) and oxygen that is attached to non-bridging network modifiers (Mg^{2+}, Ca^{2+}, the alkali metals etc. - Mysen et al., 1982). In fact, the oxygen that needs be considered is the fraction that is partitioned into the silicate via the gas phase.

The amount of oxygen that can be exchanged with a gas phase of known fO_2 is proportional to the amount of transition metals in the silicate that can have variable oxidation states. In basaltic melts this is iron. Hence, the amount of oxygen that is added to a silicate melt as fO_2 increases is proportional to the molar ratio between ferric and ferrous Fe ($X_{\mathrm{FeO}1.5}/X_{\mathrm{FeO}}$). We have computed $X_{\mathrm{FeO}_{1.5}}/X_{\mathrm{FeO}}$ as a function of fO_2 at 1300 °C using the formalism given by Kilinc et al. (1983). The resulting molar fraction of $FeO_{1.5}$ is proportional to the amount of oxygen absorbed to the silicate melt at any given fO_2 (Fig. 3.6).

At FMQ, where we have measured accurate Ru concentrations in both S-free melt and S-bearing melt, $X_{\mathrm{FeO}_{1.5}}$ in the picrite is 0.013 ($X_{\mathrm{FeO}_{1.5}}/X_{\mathrm{FeO}_{\mathrm{total}}} = 0.14$). The corresponding amount of oxygen added to the silicate melt via the gas phase is $\sim$1500 ppm. The concentration of S at FMQ and $\log fS_2 = -2.3$ in our experimental glass is 140 ppm. Hence, the O^{2-}/S^{2-} molar ratio under these conditions is 24. An alternative formalism to compute $X_{\mathrm{FeO}_{1.5}}/X_{\mathrm{FeO}}$ given by Jayasuriaya et al. (2004), gives $X_{\mathrm{FeO}_{1.5}} = 0.015$. This value cannot be distinguished within error of from the value calculated using the formalism of Kilinc et al. (1983).

The molar O^{2-}/S^{2-} ratio can now be combined with the Ru concentrations in the S-free and the S-bearing picrites. A preference factor (F) can be calculated that quantifies the extent by which Ru prefers to associate with S^{2-} over O^{2-} according to:

$$F = \frac{X_{\mathrm{O}}^{\mathrm{melt}}/X_{\mathrm{S}}^{\mathrm{melt}}}{X_{\mathrm{RuO_2}}^{\mathrm{melt}}/X_{\mathrm{RuS_2}}^{\mathrm{melt}}} \tag{3.8}$$

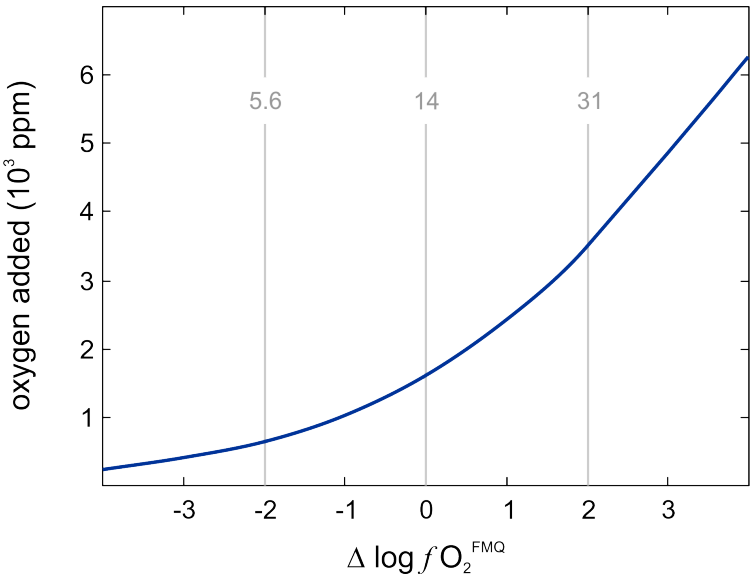

Figure 3.6: Here the amount of oxygen is shown, that is added to a silicate melt by oxidizing ferrous to ferric Fe, relative to a melt where all Fe is present as FeO. Grey lines indicate the calculated $X_{Fe_2O_3}/X_{Fe_{total}}$ (Kilinc et al., 1983) for the respective fO_2. At FMQ $\sim$1600 ppm oxygen is added, which is available to act as a ligand to Ru and the other HSE in competition to the S^{2-} ligand.

where X denote the molar fractions of O^{2-}, S^{2-}, RuO_2 and RuS_2 in the picrite. At FMQ, the Ru solubility in the S-free melt is 0.03 ± 0.01 ppm. At the same relative fO_2 in the S^{2-} -bearing melt ($\log fS_2 = -2.3$ bar), the Ru solubility is 1.0 ± 0.2 ppm. It follows that in the S-bearing silicate melt at FMQ and $\log fS_2 = -2.3$ the value of F is $\sim$1000. This value of F indicates that around 97 at.% of Ru are dissolved in the melt as RuS_2, and only 3 at.% are dissolved as RuO_2 species. The calculation clearly shows that sulfur has a major influence on Ru solubility in silicate melts contrary to the assertions by O'Neill et al. (1995). This may well be true for the other HSE as well, since that they are all characterized as chalcophile elements. However, the value of F is expected to vary depending on how chalcophile they actually are.

The above discussion is only valid up to oxygen fugacities around the FMQ-buffer. Between $\sim$FMQ+0.5 and $\sim$FMQ+1.5 sulfide is progressively oxidized to sulfate and is dissolved as SO_4^{2-} in silicate melts (e.g. Jugo et al., 2005, 2010; Metrich et al., 2009). As the sulfate/sulfide ratio in the silicate melt increases, the preference of the HSE to liaise with sulfur will rapidly diminish, because Ru is not expected to form associations with SO_4^{2-}. Under these conditions, oxygen will take over as a principal ligand to the HSE cationic species at the expense of S^{2-}, and the solubility profile of Ru, and that of the other HSE, will converge with that established for S-free melts.

3.5.2 Are basaltic melts HSE-saturated in their mantle sources?

Naldrett et al. (2008) pointed out that the abundances of HSE in some natural basalts are above the saturation level derived from experiments. At the same time, Naldrett et al. (2008) noted that these natural basalts do not contain any visible HSE alloys. He concluded that silicate magmas can carry higher HSE concentrations than what is indicated by experimental studies carried out in synthetic systems. This obvious discrepancy between observation and experiments hinges on the experimentally determined solubility limits of HSE, and might vanish if we consider the additional effect of S on HSE solubility.

For example, Borisov and Palme (2000) quote an experimentally determined Ru solubility of ~ 4 ppb in S-free silicate melts at FMQ and 1300 °C. Assuming incompatible behaviour of Ru they calculated that a magma generated by 20 % partial melting should contain 25 ppb Ru. They concluded that this magma should be oversaturated with respect to Ru. However, the Ru concentrations of natural basalts are much lower. Ocean Island Basalts (OIB) have an average abundance of 0.44 ppb Ru (Crocket, 2002). For example, the Ru abundance of primitive melts from the Canary Islands is around 0.34 ppb Ru (Day et al., 2010), whereas tholeiites from Hawaii contain slightly higher Ru concentrations of 1.2 ± 0.2 ppb (e.g. Ireland et al., 2009). All these Ru concentrations are well below the saturation limit quoted by Borisov and Palme (2000). It seems quite unrealistic to assume that these basalts should be saturated with Ru-metal. The enhancing effect of S on Ru solubility in silicate melt, which we observed in our experiments, further strengthens this argument. About 1 ppm Ru can be dissolved in the S-bearing picrite (140 ppm S). This implies that even komatiites with high Ru abundances (~ 5 ppb – Fiorentini et al., 2011) are still undersaturated with respect to Ru-metal. Sulfur most likely also influences the solubility of the other HSE in silicate melts, although it is expected that the magnitude depends on how strongly chalcophile they are. Therefore, natural basalts that typically have $\sim 1{,}000$ ppm of S are unlikely to precipitate HSE-rich alloys directly.

Rather, the formation of HSE-rich alloys is most likely due to desulfurization of mantle sulfides, either by fluid-driven metasomatism, or S-loss driven by successive episodes of partial melting, resulting in the exsolution of HSE-rich alloys from sulfides (Ballhaus and Ryan, 1995; Peregoedova et al., 2004; Fonseca et al., 2011).

3.5.3 The enrichment of HSE in magmatic sulfide ore deposits

The preference of Ru and Pd (and likely all other HSE) to associate with the S^{2-} ligand in a silicate melt has important implications for the concentration mechanisms of HSE from silicate melt into sulfide liquids and the formation of HSE-rich sulfide ore deposits, such as the Merensky and UG2 Reefs (Bushveld Complex, South Africa) or the J-M-Reef of the Stillwater Complex, USA (e.g. Ballhaus and Sylvester, 2000; Naldrett et al., 1987).

Conventionally, the transfer of the noble metals from a primitive silicate melt into an immiscible sulfide melt is quantified by the R-factor model (Campbell et al., 1979). In this model, the HSE tenor of a sulfide melt is a function of three parameters: (1) the sulfide-silicate partition coefficient ($D_{\mathrm{HSE}}^{\mathrm{sulfide-silicate}}$), (2) the HSE concentration in silicate melt, and (3) the amount of silicate melt with which a given amount of sulfide melt is equilibrated. This latter mass ratio is known in the literature as the R-factor (Campbell and Naldrett, 1979). For a detailed discussion see Campbell et al. (1983) and Naldrett et al. (1986).

By not specifying how the HSE are dissolved in silicate melt, the R-factor model implies that the HSE species in silicate would need to establish the direct physical contact with exsolved sulfide, in order to become enriched in the sulfide melt. If the HSE are preferentially associated with S^{2-} in sulfide-undersaturated silicate melt, as shown by our experiments, then sulfide exsolution alone will cause HSE enrichment, if the exsolution of a sulfide melt is defined as the collection of all metal-S molecules in silicate melt into a new phase (immiscible sulfide melt - Fig. 3.7). Complex mixing scenarios, as proposed by Campbell et al. (1983) to achieve high R-factors, are unnecessary to concentrate the HSE into the sulphide droplets.

In order to demonstrate this, one can estimate the Ru concentration of sulfide exsolving from the silicate melt using the preference factor as defined by Eq. 3.8. From the Ru experiment at FMQ and $\log fS_2 = -2.3$, with ~ 1 ppm Ru and 140 ppm S^{2-} (i.e. RU54 in Table 3.1) and a preference factor of $F = 1000$ (Eq. 3.8), we calculated that 97 at.% of Ru in picrite is present as RuS_2 species and 3 at.% as RuO_2 species (cf. chapter 3.5.1). The Ru concentration of an exsolving sulfide liquid that exsolves from this silicate melt can then be calculated assuming for simplicity that (1) all RuS_2 molecules are sequestered into the sulphide melt (2) all remaining S in the silicate melt (i.e. the portion that is not attached to Ru) is associated

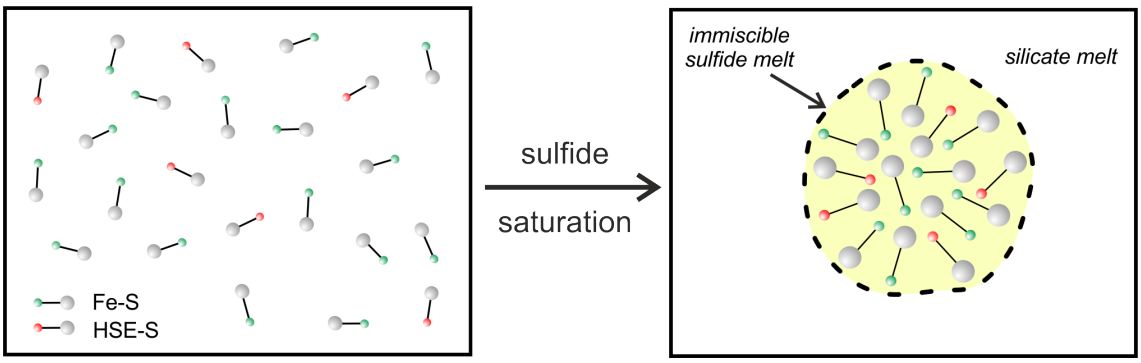

Figure 3.7: Cartoon illustrating the transfer of chalcophile elements from a silicate melt to an exsolving sulfide liquid. In the S-undersaturated silicate melt chalcophile elements such as the HSE or Fe are present associated with the S^{2-}-ligand. When sulfide saturation is triggered, all these metals are automatically transferred to the newly forming sulfide melt.

with Fe only (3) Ru and Fe enter the sulfide melt in the same proportions as they are attached to sulfur in the silicate melt. This simple calculation yields a sulfide melt that would contain 0.26 wt.% Ru and the remainder being Fe and S. Obviously, this calculated Ru concentration in the hypothetical sulfide is orders of magnitude higher than what is observed in naturally occurring sulfides (e.g. 35 ppm in Merenksy sulfides – Naldrett et al. 1986). However, our experiments are saturated with Ru-metal, so that the Ru concentration in the silicate melt of our experiments is at its maximum, which is orders of magnitude higher than what is observed in basaltic melts. The same would be true at sulfide saturation, because Ru concentrations in the silicate and sulfide melts would be buffered by the Ru-metal, i.e. would me maximal.

In a magma chamber the situation is different, because no metal is stable and the magma defines a finite reservoir with a Ru concentration in the lower ppb range. Therefore, we repeated the above calculation now using the composition of the parental magma of the Merensky Reef (Davies and Tredoux, 1985) as a starting point. This melt contains an average of 6 ppb Ru and 518 ppm S. Using the preference factor $F = 1000$ and assuming that no external S was added, we calculate that the sulfide liquid should contain 42 ppm Ru, which compares well with the measured concentration of 35 ppm.

Obviously our calculation is very simplistic in that the assumptions outlined above are used. Nevertheless, it illustrates well that a sulfide melt may be highly enriched in Ru and possibly the other HSE from the onset of sulfide saturation. A mechanical

exposure of sulfide droplets to fresh silicate melt, in order to equilibrate with a large volume of silicate, as proposed in the R-factor model, is unnecessary to concentrate the HSE into the sulfide droplets. A sulfide droplet in a rapidly quenched MORB glass (e.g. Peach et al., 1994) may contain as much HSE as a sulfide droplet in the Merensky reef (e.g. Ballhaus et al. 2006).

3.6 Summary and conclusions

The results of this study show that the solubility of Ru is enhanced by more than one order of magnitude when S^{2-} is available as a ligand to Ru under sulfide undersaturated conditions, compared to the S-free system. The results of our experiments contribute to an improved understanding of solubility mechanisms of HSE in silicate melts. Ruthenium, and possibly other HSE as well, do not only dissolve in silicate melts as oxides, as is the classical assumption. Rather, Ru is shown to be 1000 times more likely to associate with S^{2-} than with O^{2-} (at FMQ and $\log fS_2 = -2.3$ bar). This clearly shows that sulfur has a major control on Ru solubility in silicate melts, and possibly also other HSE as well.

The finding that Ru associates with S^{2-} as a ligand in silicate melts has important implications for our understanding of HSE enrichment in sulfide liquids. Our proposed model works also in static systems, where sulfide droplets do not have the chance to equilibrate with "fresh" silicate melt after their formation. For example, sulfide droplets in MORB glasses also show highly enriched HSE concentrations (e.g. Peach et al., 1994), which can be nicely explained by our model.

4 References

Alard O., Griffin W. L., Lorand J. P., Jackson S. E. and O'Reilly S. Y. (2000) Non-chondritic distribution of the highly siderophile elements in mantle sulphides. *Nature* **407**, 891–894.

Alard O., Luguet A., Pearson N. J., Griffin W. L., Lorand J.-P., Gannoun A., Burton K. W. and O'Reilly S. Y. (2005) In situ Os isotopes in abyssal peridotites bridge the isotopic gap between MORBs and their source mantle. *Nature* **436**, 1005–1008.

Andrews D. R. A. and Brenan J. M. (2002a) Phase-equilibrium constraints on the magmatic origin of laurite plus Ru-Os-Ir alloy. *Canadian Mineralogist* **40**, 1705–1716.

Andrews D. R. A. and Brenan J. M. (2002b) The solubility of ruthenium in sulfide liquid: Implications for platinum group mineral stability and sulfide melt-silicate melt partitioning. *Chemical Geology* **192**, 163–181.

Arculus, R. J. and Delano, J. W.(1981) Siderophile element abundances in the upper mantle: evidence for a sulphide signature and equilibrium with the core. *Geochimica et Cosmochimica Acta* **45**, 1331-1343.

Ballhaus C. and Ryan C. G. (1995). Platinum-group elements in the Merensky Reef I. PGE in solid solution in base metal sulfides and the down temperature equilibration of Merensky ores. *Contributions to Mineralogy and Petrology* **122**, 241–251

Ballhaus C. and Sylvester P. J. (2000). Noble metal processes in the Merensky Reef, Bushveld complex. *Journal of Petrology* **41**, 545–561

Ballhaus C., Tredoux M. and Spath A. (2001) Phase relations in the Fe-Ni-Cu-PGE-S system at magmatic temperature and application to massive sulphide ores of the Sudbury Igneous Complex. *Journal Of Petrology* **42**, 1911–1926.

Ballhaus C., Bockrath C., Wohlgemuth-Ueberwasser C., Laurenz V. and Berndt J. (2006) Fractionation of the noble metals by physical processes. *Contributions to Mineralogy and Petrology* **152**, 667–684.

Barnes S.-J., Naldrett A. J. and Gorton M. P. (1985) The origin of platinum-group elements in terrestrial magmas. *Chemical Geology* **53**, 303–323.

Barnes S. J., Boyd R., Korneliussen A., Nilsson L. P., Often M., Pedersen R. B. and Robins B. (1988) The use of mantle normalization and metal ratios in discriminating between the effects of partial melting, crystal fractionation, and sulphide segregation on platinum-group elements, gold, nickel, and copper: examples from Norway. In: *Geoplatinum* (eds. H. M. Prichard, P. J. Potts, S. J. Bowles and S. J. Cripp). Elsevier, Amsterdam, pp. 113–143.

Barnes S. J. and Fiorentini M. L. (2008) Iridium, ruthenium and rhodium in komatiites: Evidence for iridium alloy saturation. *Chemical Geology* **257**, 44–58

Becker H., Shirey S. B. and Carlson R. W. (2001) Effects of melt percolation on the Re–Os systematics of peridotites from a Paleozoic convergent plate margin. *Earth and Planetray Science Letters* **188**, 107–121.

Becker H., Horan M. F., Walker R. J., Gao S., Lorand J.-P. and Rudnick R. L. (2006) Highly siderophile element composition of the Earth's primitive upper mantle: Constraints from new data on peridotite massifs and xenoliths. *Geochimica et Cosmochimica Acta* **70**, 4528–4550.

Bezmen N. I., Asif M., Brügmann G. E., Romanenko I. M. and Naldrett A. J. (1994) Distribution of Pd, Rh, Ru, Ir, Os, and Au between sulfide and silicate metals. *Geochimica et Cosmochimica Acta* **58**, 1251–1260.

Bezos A., Lorand J.-P., Humler E. and Gros M. (2005) Platinum-group element systematics in Mid-Oceanic Ridge basaltic glasses from the Pacific, Atlantic, and Indian Oceans. *Geochimica et Cosmochimica Acta* **69**, 2613–2627.

Bockrath C., Ballhaus C. and Holzheid A. (2004a) Fractionation of the platinum-group-elements during mantle melting. *Science* **305**, 1951–1953.

Bockrath C., Ballhaus C. and Holzheid A. (2004b) Stabilities of laurite RuS2 and monosulfide liquid solution at magmatic temperature. *Chemical Geology* **208**, 265–271.

Borisov A., Palme H. and Spettel B. (1994) Solubility of Pd in silicate melts: Implications for core formation in the Earth. *Geochimica et Cosmochimica Acta* **58**, 705–716.

Borisov A. and Danyushevsky L. (2011) The effect of silica contents on Pd, Pt and Rh solubilities in silicate melts: an experimental study. *European Journal of Mineralogy* 23, 355–367.

Borisov A. and Nachtweyh K. (1998) Ru solubility in silicate melts: experimental results in oxidizing region. *Lunar and Planetary Science Conference* **XXIX**, 1320.

Borisov A. and Palme H. (1995) The solubility of iridium in silicate melts: New data from experiments with $Ir_{10}Pt_{90}$ alloys. *Geochimica et Cosmochimica Acta* **59**, 481–485.

Borisov A. and Palme H. (1996) Experimental determination of the solubility of Au in silicate melts. *Mineralogy and Petrology* **56**, 297–312.

Borisov A. and Palme H. (1997) Experimental determination of the solubility of platinum in silicate melts. *Geochimica et Cosmochimica Acta* **61**, 4349–4357.

Borisov A. and Palme H. (2000) Solubilities of noble metals as derived from experiments in Fe-free systems. *American Mineralogist* **85**, 1665–1673.

Borisov A., Lahaye Y. and Palme H. (2004) The effect of TiO_2 on Pd, Ni and Fe solubilities in silicate melts. *American Mineralogist* **89**, 564–571.

Botcharnikov R. E., Linnen R. L., Wilke M., Holtz F., Jugo P. J. and Berndt J. (2011) High gold concentrations in sulphide-bearing magma under oxidizing conditions. *Nature Geoscience* **4**, 112–115.

Brandon A. D., Norman M. D., Walker R. J. and Morgan J. W. (1999) ^{186}Os–^{187}Os systematics of Hawaiian picrites. *Earth and Planetray Science Letters* **174**, 25–42.

Brandon A. D. and Walker R. J. (2005) The debate over core–mantle interaction. *Earth and Planetray Science Letters* **232**, 211–225.

Brenan J. M., McDonough, W. F. and Dalpe, C. (2003) Experimental constraints on the partitioning of rhenium and some platinum group elements between olivine and silicate melt. *Earth and Planetary Science Letters* **212**, 135–150.

Brenan J. M. (2008) Re-Os fractionation by sulfide melt-silicate melt partitioning: A new spin. *Chemical Geology* **248**, 140–165.

Brenan J. M. and McDonough W. F. (2009) Core formation and metal-silicate fractionation of osmium and iridium from gold. *Nature Geoscience* **2**, 798–801.

Campbell I. H. and Naldrett A. J. (1979) Influence of Silicate-Sulfide Ratios on the Geochemistry of Magmatic Sulfides. *Economic Geology* **74**, 1503–1506.

Campbell I. H., Naldrett A. J. and Barnes S. J. (1983) A Model for the Origin of the Platinum-Rich Sulfide Horizons in the Bushveld and Stillwater Complexes. *Journal of Petrology* **24**, 133–165.

Capobianco C. J., Jones J. H. and Drake M. J. (1993) Metal-silicate thermochemistry at high temperature: magma oceans and "the excess siderophile element" problem of the Earth's upper mantle. *Journal of Geophysical Research* **98**, 5433–5443.

Capobianco C. J. and Hervig R. L. (1996) Solubility of Ru and Pd in silicate melts: The effect of melt composition. *Lunar and Planetary Science Conference* **XXVII**, 197–198 (abstr.).

Caroll M. R. and Rutherford M. J. (1985) Sulfide and sulfate saturation in hydrous silicate melts. *Journal of Geophysical Research* **90**, C601–C612.

Carroll M. R. and Rutherford M. J. (1988) Sulfide speciation in hydrous experimental glasses of varying oxidation state: results from measured wavelength shifts of sulfur X-rays. *American Mineralogist* **73**, 845–849.

Chase M. W. (1998) *NIST-JANAF Thermodynamic Tables.* National Institute of Standards and Technology, Washington DC, USA.

Chou C. L. (1978) Fractionation of siderophile elements in the Earth's upper mantle. *Proceedings of the Lunar Science Conference* **88**, 507–518.

Cottrell E. and Walker D. (2002) A New Look at Pt Solubility in Silicate Liquid. *Lunar and Planetary Science Conference* **XXXIII**, abstract no. 1274.

Cottrell E. and Walker D. (2006) Constraints on core formation from Pt partitioning in mafic silicate liquids at high temperatures. *Geochimica et Cosmochimica Acta* **70**, 1565–1580.

Crocket J. H. (2002) Platinum-group element geochemistry of mafic and ultramafic rocks. In: *The Geology, Geochemistry, Mineralogy and mineral beneficiation of Platinum-group elements, Special Volume* **54** (ed. L. J. Cabri). Canadian Institute of Mining, Metallurgy and Petroleum, pp. 177–210.

Davies G. and Tredoux M. (1985) The platinum-group element and gold contents of the marginal rocks and sills of the Bushveld Complex. *Economic Geology* **80**, 838–848.

Day J. M. D., Pearson D. G., Macpherson C. G., Lowry D. and Carracedo J. C. (2010) Evidence for distinct proportions of subducted oceanic crust and lithosphere in

HIMU-type mantle beneath El Hierro and La Palma, Canary Islands. *Geochimica et Cosmochimica Acta* **74**, 6565–6589.

Drake M. J. and Righter K. (2002) Determining the composition of the Earth. *Nature* **416**, 39–44.

Ertel W., O'Neill H. St. C., Sylvester P. J. and Dingwell D. B. (1999) Solubility of Pt and Rh in haplobasaltic silicate melt at 1300 ℃. *Geochimica et Cosmochimica Acta* **60**, 1171–1180.

Ertel W., O'Neill H. St. C., Sylvester P. J., Dingwell D. B. and Spettel B. (2001) The solubility of Rhenium in silicate melts: Implications for the geochemical properties of rhenium at high temperatures. *Geochimica et Cosmochimica Acta* **65**, 2161–2170.

Ertel W., Walter M. J., Drake M. J. and Sylvester P. J. (2006) Experimental study of platinum solubility in silicate melt to 14 GPa and 2273 K: Implications for accretion and core formation in Earth. *Geochimica et Cosmochimica Acta* **70**, 2591–2602.

Ertel W., Dingwell D. B. and Sylvester P. J. (2008) Siderophile elements in silicate melts — a review of the mechanically assisted equilibration technique and the nanonugget issue. *Chemical Geology* **248**, 119–139.

Evans K. A., O'Neill H. St. C. and Mavrogenes J. A. (2008) Sulphur solubility and sulphide immiscibility in silicate melts as a function of the concentration of manganese, nickel, tungsten and copper at 1 atm and 1400 ℃. *Chemical Geology* **255**, 236–249.

Fiorentini M. L., Barnes S. J., Maier W. D., Burnham O. M. and Heggie G. (2011) Global Variability in the Platinum-group Element Contents of Komatiites. *Journal of Petrology* **52**, 83–112.

Fleet M.E., Chryssoulis S.L., Szone W.E. and Weisener C.G. (1993) Partitioning of platinum-group elements and Au in the Fe-Ni-Cu-S system – experiments on the fractional crystallization of sulfide melt. *Contributions to Mineralogy and Petrology* **115**, 36-44.

Fleet M. E., Crocket J. H. and Stone W. E. (1996) Partitioning of platinum-group elements (Os, Ir, Ru, Pt, Pd) and gold between sulfide liquid and basalt melt. *Geochimica et Cosmochimica Acta* **60**, 2397–2412.

Fleet M. E., Liu M. and Crocket J. H. (1999) Partitioning of trace amounts of highly siderophile elements in the Fe-Ni-S system and their fractionation in nature. *Geochimica et Cosmochimica Acta* **63**, 2611–2622.

Fonseca R. O. C., Mallmann G., O'Neill H. S. C. and Campbell I. H. (2007) How chalcophile is rhenium? An experimental study of the solubility of Re in sulphide mattes. *Earth and Planetary Science Letters* **260**, 537–548.

Fonseca R. O. C., Campbell I. H., O'Neill H. St. C. and Allen C. (2009) Solubility of Pt in sulphide mattes: Implications for the genesis of PGE-rich horizons in layered intrusions. *Geochimica et Cosmochimica Acta* **73**, 5764–5777.

Fonseca R. O. C., Mallmann G., O'Neill H. St. C., Campbell I. H. and Laurenz V. (2011) Solubility of Os and Ir in sulfide melt: Implications for Re/Os fractionation during partial melting. *Earth and Planetary Science Letters* **311**, 339–350.

Fortenfant S. S., Günther D., Dingwell D. B. and Rubie D. C. (2003) Temperature dependence of Pt and Rh solubilities in a haplobasaltic melt. *Geochimica et Cosmochimica Acta* **67**, 123–131.

Fortenfant S. S., Dingwell D. B., Ertel-Ingrisch W., Capmas F., Birck J. L. and Dalpe C. (2006) Oxygen fugacity dependence of Os solubility in haplobasaltic melt. *Geochimica et Cosmochimica Acta* **70**, 742–756.

Handler M. R. and Bennett V. C. (1999) Behaviour of Platinum-group elements in the subcontinental mantle of eastern Australia during variable metasomatism and melt depletion. *Geochimica et Cosmochimica Acta* **63**, 3597–3618.

Hart S. R. and Ravizza G. E. (1996) Os partitioning between phases in lherzolite and basalt. In: *Earth processes: Reading the isotopic code*, *Geophysical Monograph Series* **95** (eds. A. Basu and S. R. Hart), pp. 123–134.

Harvey J., Dale C. W., Gannoun A. and Burton K. W. (2011) Osmium mass balance in peridotite and the effects of mantle-derived sulphides on basalt petrogenesis. *Geochimica et Cosmochimica Acta* **75**, 5574–5596.

Helmy H. M., Ballhaus C., Berndt J., Bockrath C. and Wohlgemuth-Ueberwasser C. (2007) Formation of Pt, Pd and Ni tellurides: experiments in sulfide-telluride systems. *Contributions to Mineralogy and Petrology* **153**, 577–591.

Helmy H. M., Ballhaus C., Wohlgemuth-Ueberwasser C., Fonseca, R. O. C. and Laurenz, V. (2010) Partitioning of Se, As, Sb, Te and Bi between monosulfide solid

solution and sulfide melt – application to magmatic sulfide deposits. *Geochimica et Cosmochimica Acta* **74**, 6174–6179.

Hillgren V. J., Drake M. J. and Rubie D. C. (1996) High pressure and high temperature metal-silicate partitioning of siderophile elements: The importance of silicate liquid composition. *Geochimica et Cosmochimica Acta* **60**, 2257–2263.

Holzheid A., Sylvester P., O'Neill H. St. C., Rubie D. C. and Palme H. (2000) Evidence for a late chondritic veneer in the Earth's mantle from high-pressure partitioning of palladium and platinum. *Nature* **406**, 396–399.

Ireland T. J., Walker R. J. and Garcia M. O. (2009) Highly siderophile element and ^{187}Os isotope systematics of Hawaiian picrites: Implications for parental melt composition and source heterogeneity. *Chemical Geology* **260**, 112–128.

Jagoutz E., Palme H., Baddenhausen H., Blum K. and Cendales M. (1979) The abundances of major, minor and trace elements in the Earth's mantle as derived from primitive ultramafic nodules. *Proceedings of the Lunar and Planetary Science Conference* **10**, 2031-2050.

Jana D. and Walker D. (1997a) The influence of sulfur on partitioning of siderophile elements. *Geochimica et Cosmochimica Acta* **61**, 5255–5277.

Jana D. and Walker D. (1997b) The influence of silicate melt composition on distribution of siderophile elements among metal and silicate liquids. *Earth and Planetary Science Letters* **150**, 463–472.

Jarosewich E., Nelen J. A. and Norberg J. A. (1980) Reference samples for electron microprobe analysis. *Geostandards Newsletter* **4**, 43–47.

Jayasuriya K. D., O'Neill H. S., Berry A. J. and Campbell S. J. (2004) A Mossbauer study of the oxidation state of Fe in silicate melts. *American Mineralogist* **89**, 1597–1609.

Jégo S., Pichavant M. and Mavrogenes J. A. (2010) Controls on gold solubility in arc magmas: An experimental study at 1000 °C and 4 kbar. *Geochimica et Cosmochimica Acta* **74**, 2165–2189.

Jégo S. and Pichavant M. (in press) Gold solubility in arc magmas: Experimental determination of the effect of sulfur at 1000 °C and 0.4 GPa. *Geochimica et Cosmochimica Acta*.

Jochum K. P., Stoll B., Herwig K., Willbold M., Hofmann A. W. (2006) MPI-DING reference glasses for in situ microanalysis: New reference values for element concentrations and isotope ratios. *Geochemistry, Geophysics, Geosystems* **7**,Q02008. doi:10.1029/2005GC001060.

Jochum K. P., Weis, U., Stoll, B., Kuzmin, D., Yang, Q., Raczek, I., Jacob, D. E., Stracke, A., Birbaum, K., Frick, D. A., Günther, D. and Enzweiler, J. (2011), Determination of reference values for NIST SRM 610-617 glasses following ISO guidelines. *Geostandards and Geoanalytical Research*, doi: 10.1111/j.1751-908X.2011.00120.x.

Johnson Matthey Base Price (www.platinum.matthey.com) retreived 2. February 2012.

Jones J. H. and Drake M. J. (1986) Geochemical constraints on core formation in the Earth. *Nature* **322**, 221–228.

Jugo P. J., Luth R. W. and Richards J. P. (2005) Experimental data on the speciation of sulfur as a function of oxygen fugacity in basaltic melts. *Geochimica et Cosmochimica Acta* **69**, 497–503.

Jugo P. J. (2009) Sulfur content at sulfide saturation in oxidized magmas. *Geology* **37**, 415–418.

Jugo P. J., Wilke M. and Botcharnikov R. E. (2010) Sulfur K-edge XANES analysis of natural and synthetic basaltic glasses: Implications for S speciation and S content as function of oxygen fugacity. *Geochimica et Cosmochimica Acta* **74**, 5926–5938.

Keays R. R. (1995) The Role of Komatiitic and Picritic Magmatism and S-Saturation in the Formation of Ore-Deposits. *Lithos* **34**, 1–18.

Kilinc A., Carmichael I. S. E., Rivers M. L. and Sack R. O. (1983) The ferric-ferrous ratio of natural silicate liquids equilibrated in air. *Contributions to Mineralogy and Petrology* **83**, 136–140.

Kimura K., Lewis R. S. and Anders E. (1974) Distribution of gold and rhenium between nickel-iron and silicate melts: implications for the abundance of siderophile elements on the Earth and Moon. *Geochimica et Cosmochimica Acta* **38**, 683–701.

Klimm K. and Botcharnikov R. E. (2010) The determination of sulfate and sulfide species in hydrous silicate glasses using Raman spectroscopy. *American Mineralogist* **95**, 1574–1579.

Kohn S. C. and Schofield P. F. (1994) The importance of melt composition in controlling trace-element behaviour: an experimental study of Mn and Zn partitioning between forsterite and silicate melts. Chemical Geology 117(1-4), 73-87.

Kress V. C., Ghiorso M. S. and Lastuka C. (2004) Microsoft EXCEL spreadsheet-based program for calculating equilibrium gas speciation in the C-O-H-S-Cl-F system. *Computers & Geosciences* **30**, 211–214.

Laurenz V., Ballhaus C., O'Neill H. St. C., Wohlgemut-Ueberwasser C. C. and Fonseca R. O. C. (2009) Ir partitioning between chromite and silicate melt — The influence of fO_2. *Geochimica et Cosmochimica Acta* **73**, Supplement S, A727.

Laurenz V., Fonseca R. O. C., Ballhaus C. and Sylvester P. J. (2010) Solubility of palladium in picritic melts: 1. The effect of iron. *Geochimica et Cosmochimica Acta* **74**, 2989–2998.

Li C., Ripley E. M. and Mathez E. A. (2003) The effect of S on the partitioning of Ni between olivine and silicate melt in MORB. *Chemical Geology* **201**, 295–306.

Lorand J.-P. and Alard O. (2001) Platinum-group element abundances in the upper mantle: new constraints from in situ and whole-rock analyses of Massif Central xenoliths (France). *Geochimica et Cosmochimica Acta* **65**, 2789–2806.

Lorand J.-P., Pattou L. and Gros M. (1999) Fractionation of platinum-group elements and gold in the upper mantle: a detailed study in Pyrenean orogenic lherzolites. *Journal of Petrology* **40**, 957–981.

Lorand J.-P., Luguet A. and Alard O. (2008) Platinum-group elements: a new set of key tracers for the Earth's Interior. *Elements* **4**, 247–252.

Lorand J.-P., Alard O. and Luguet A. (2010) Platinum-group element micronuggets and refertilization process in Lherz orogenic peridotite (northeastern Pyrenees, France). *Earth and Planetary Science Letters* **289**, 298-310.

Luguet A., Lorand J.-P. and Seyler M. (2003) Sulfide petrology and highly siderophile element geochemistry of abyssal peridotites: a coupled study of samples from the Kane Fracture Zone (45°W 23°20'N, MARK area, Atlantic Ocean). *Geochimica et Cosmochimica Acta* **67**, 1553–1570.

Luguet A., Lorand J.-P., Alard O. and Cottin J.-Y. (2004) A multi-technique study of platinum group element systematic in some Ligurian ophiolitic peridotites, Italy. *Chemical Geology* **208**, 175–194.

Luguet A., Shirey S. B., Lorand J. P., Horan M. F. and Carlson R. W. (2007) Residual platinum-group minerals from highly depleted harzburgites of the Lherz massif (France) and their role in HSE fractionation of the mantle. *Geochimica et Cosmochimica Acta* **71**, 3082–3097.

Luguet A., Pearson D. G., Nowell G. M., Dreher S. T., Coggon J. A., Spetsius Z. V. and Parman S. W. (2008) Enriched Pt-Re-Os isotope systematics in plume lavas explained by metasomatic sulfides. *Science* **319**, 453–456.

Makovicky E., Karup-Møller S., Makovicky M. and Rose-Hansen J. (1990) Experimental studies on the phase systems Fe-Ni-Pd-S and Fe-Pt-Pd-As-S applied to PGE deposits. *Mineralogy and Petrology* **42**, 307–319.

Mallmann G. and O'Neill H. St. C. (2007) The effect of oxygen fugacity on the partitioning of Re between crystals and silicate melt during mantle melting. *Geochimica et Cosmochimica Acta* **71**, 2837–2857.

Mann U., Frost D. J. and Rubie D. C. (in press) Evidence for high-pressure core-mantle differentiation from the metal-silicate partitioning of lithophile and weakly siderophile elements. *Geochimica et Cosmochimica Acta*.

Mavrogenes J. A. and O'Neill H. S. C. (1999) The relative effects of pressure, temperature and oxygen fugacity on the solubility of sulfide in mafic magmas. *Geochimica et Cosmochimica Acta* **63**, 1173–1180.

Médard E., Schmidt M. W., Wähle M., Keller N. S. and Günther D. (2010) Pt in silicate melts: Centrifuging nanonuggets to decipher core formation processes. *Lunar and Planetary Science Conference* **XXXXI**, #2639 (abstr.).

Mitchell R. H. and Keays R. R. (1981) Abundance and Distribution of Gold, Palladium and Iridium in Some Spinel and Garnet Iherzolites — Implications for the Nature and Origin of Precious Metal-Rich Intergranular Components in the Upper Mantle. *Geochimica et Cosmochimica Acta* **45**, 2425–2442.

Morgan J. W., Wandless G. A., Petrie R. K. and Irving A. J. (1981) Composition of the Earths Upper Mantle. 1. Siderophile Trace-Elements in Ultramafic Nodules. *Tectonophysics* **75**, 47–67.

Morgan J. W., Walker R. J., Brandon A. D. and Horan M. F. (2001) Siderophile elements in the Earth's upper mantle and lunar breccias: data synthesis suggests manifestations of the same late influx. *Meteoritics and Planetary Science* **36**, 1257–1275.

Mungall J. E., Andrews D. R. A., Cabri L. J., Sylvester P. J. and Tubrett M. (2005) Partitioning of Cu, Ni, An, and platinum-group elements between monosulfide solid solution and sulfide melt under controlled oxygen and sulfur fugacities. *Geochimica et Cosmochimica Acta* **69**, 4349–4360.

Mungall J. E. and Su S. (2005) Interfacial tension between magmatic sulfide and silicate liquids: Constraints on kinetics of sulfide liquation and sulfide migration through silicate rocks. *Earth and Planetary Science Letters* **234**, 135–149.

Mungall J. E. and Naldrett A. J. (2008) Ore Deposits of the Platinum-Group Elements. *Elements* **4**, 253–258.

Murthy V. (1991) Early differentiation of the Earth and the problem of mantle siderophile elements: A new approach. *Science* **253**, 303–306.

Mysen B. O., Virgo D. and Seifert F. A. (1982) The structure of silicate melts: Implications for chemical and physical properties of natural magma. *Reviews of Geophysics and Space Physics* **20**, 353–383.

Naldrett A. J. (2004) *Magmatic sulfide deposits: Geology, geochemistry and Exploration.* Springer-Verlag, Berlin-Heidelberg.

Naldrett A. J., Cameron G., von Gruenewald G. and Sharpe M. R. (1987). The formation of stratiform PGE deposits in layered intrusions. In: *Origins of Igenous Layering* (ed. I. Parsons). *NATO advanced Science Institute Series C* **196**, pp. 313–397.

Naldrett A. J., Fedorenko V. A., Asif M., Shushen L., Kunilov V. E., Stekhin A. I., Lightfoot P. C. and Gorbachev N. S. (1996) Controls on the composition of Ni-Cu sulfide deposits as illustrated by those at Noril'sk, Siberia. *Economic Geology and the Bulletin of the Society of Economic Geologists* **91**, 751–773.

Naldrett A. J., Kinnaird J., Wilson A. and Chunnett, G. Concentration of PGE in the Earth's Crust with special reference to the Bushveld Complex (2008). *Earth Science Frontiers* **15**, 264–297.

Naldrett A. J. (2010) Secular variations of magmatic sulfide deposits and their source magmas. *Economic Geology* **105**, 669–688.

Newsom H. E. (1990) Accretion and core formation in the Earth: evidence from siderophille elements. In: *Origin of the Earth* (eds. H. E. Newsom and J. H. Jones). Oxford University Press, pp. 273–288

O'Neill H. St. C. (1987) Quartz-fayalite-iron and quartz-fayalite-magnetite equilibria and the free energies of formation of fayalite (Fe_2SiO_4) and magnetite (Fe_3O_4). *American Mineralogist* **72**, 67–75.

O'Neill H. St. C. (1991) The origin of the Moon and the early history of the Earth — A chemical model Part 2: The Earth. *Geochimica et Cosmochimica Acta* **55**, 1159–1172.

O'Neill H. St. C., Dingwell D. B., Borisov A., Spettel B. and Palme H. (1995) Experimental petrochemistry of some highly siderophile elements at high temperatures, and some implications for core formation and the mantle's early history. *Chemical Geology* **120**, 255–273.

O'Neill H. St. C. and Eggins S. M. (2002) The effect of melt composition on trace element partitioning: an experimental investigation on the activity coefficients of FeO, NiO, CoO, MoO_2 and MoO_3. *Chemical Geology* **186**, 151–181.

O'Neill H. St. C. and Mavrogenes J. A. (2002) The sulfide capacity and the sulfur content at sulfide saturation of silicate melts at 1400 ℃ and 1 bar. *Journal of Petrology* **43**, 1049–1087.

Palme H. and Jones A. (2003) Solar system abundances of the elements. In: *Treatise on geochemistry Vol. 1* (ed. A.M. Davis). Elsevier, Amsterdam, p 41–61.

Palme H. and O'Neill H. St. C. (2003) Cosmochemical estimates of mantle composition. In: *Treatise on geochemistry 2* (ed. R.W. Carlson). Elsevier, Amsterdam, pp. 1–38.

Palme H. (2008) Platinum-Group Elements in Cosmochemistry. *Elements* **4**, 233–238.

Peach C. L., Mathez E. A. and Keays R. R. (1990) Sulfide melt-silicate melt distribution coefficients for noble metals and other chacophile elements as deduced from MORB: Implications for partial melting. *Geochimica et Cosmochimica Acta* **54**, 3379–3389.

Peach C. L., Mathez E. A., Keays R. R. and Reeves S. J. (1994) Experimentally determined sulfide melt-silicate melt partition coefficients for iridium and palladium. *Chemical Geology* **117**, 361–377.

Pearson D. G., Alard O., Griffin W. L., Jackson S. E. and O'Reilly S. Y. (2002) In situ measurement of Re-Os isotopes in mantle sulphides by laser-ablation multicollector inductively cpupled plasma mass spectromety: analytical methods and preliminary results. *Geochimica et Cosmochimica Acta* **66**, 1037–1050.

Pearson D. G., Irvine G. J., Ionov D. A., Boyd F.R. and Dreibus G. E. (2004), Re-Os isotope systematics and platinum-group element fractionation during mantle melt extraction: a study of massif and xenolith peridotite suites. *Chemical Geology* **208**, 29–59.

Peregoedova A., Barnes S.-J., Baker, D. R., (2004). The formation of Pt- Ir alloys and Cu-Pd-rich sulfide melts by partial desulfurization of Fe-Ni-Cu sulfides: results of experiments and implications for natural systems. *Chemical Geology* **208**, 247–264.

Peucker-Ehrenbrink B. and Jahn B.-M. (2001) Rhenium-osmium isotope systematics and platinum group element concentations: loess and the upper continental crust. *Geochemestry Geophysics and Geosystems* **2**, 2001GC000172.

Philipp H., Eckhardt J. D. and Puchelt H. (2001) Platinum-group elements (PGE) in basalts of the seaward-dipping reflector sequence, SE Greenland coast. *Journal of Petrology* **42**, 407–432.

Puchtel I., Brandon A. D., Humayun M. and Walker R. J. (2005) Evidence for the early differentiation of the core from Pt–Re–Os isotope systematics of 2.8-Ga komatiites. *Earth and Planetray Science Letters* **237**, 118–134.

Pruseth, K. L., Palme, H., 2004. The solubility of Pt in liquid Fe-sulfides. *Chemical Geology* **208**, 233–245.

Rehkämper M., Halliday A. N., Fitton J. G., Lee D. C., Wieneke M. and Arndt N. T. (1999) Ir, Ru, Pt, and Pd in basalts and komatiites: New constraints for the geochemical behavior of the platinum-group elements in the mantle. *Geochimica et Cosmochimica Acta* **63**, 3915–3934.

Righter K. and Drake M. J. (1997) Metal-silicate equilibrium in a homogeneously accreting earth: New results for Re. Earth and Planetary Science Letters **146**, 541–553.

Righter K., Humayun M. and Danielson L (2008) Partitioning of palladium at high pressures and temperatures during core formation. *Nature Geoscience* **1**, 321–323.

Ringwood A. E., (1979) *Origin of the Earth and Moon.* Springer-Verlag, Berlin.

Rohrbach A., Schuth S., Ballhaus C., Münker C., Matveev S. and Qopoto C. (2005) Petrological Constraints on the origin of arc Picrites, New Georgia Group, Solomon Islands. *Contributions to Mineralogy and Petrology* **149**, 685–698.

Rose-Weston L., Brenan J. M., Fei Y., Secco R. A. and Frost D. J. (2009) Effect of pressure, temperature, and oxygen fugacity on the metal-silicate partitioning of Te, Se, and S: Implications for earth differentiation. *Geochimica et Cosmochimica Acta* **73**, 4598–4614.

Rudnick R. L. and Gao S. (2003) Composition of the continental crust. In: *Treatise on Geochemistry 3* (ed R. L. Rudnick). Elsevier, Amsterdam, pp. 1–56.

Schmidt M. W., Connolly J. A. D., Günther D. and Bogaerts M. (2006) Element Partitioning: The Role of Melt Structure and Composition. *Science* **312**, 1646–1650.

Schuth S., Rohrbach A., Münker C., Ballhaus C., Garbe-Schönberg D. and Qopoto C. (2004) Geochemical constraints on the petrogenesis of arc picrites and basalts, New Georgia Group, Solomon Islands. *Contributions to Mineralogy and Petrology* **148**, 288–304.

Simon A. C. and Ripley E. M. (2011) The role of magmatic sulfur in the formation of ore deposits. In: *Sulfur in magmas and melts: Its importance for natural and technical processes*, *Reviews in Mineralogy and Geochemistry* **73** (ed. H. Behrens and J. D. Webster). Mineralogical Society of America, pp. 513–578.

Snow J. E. and Schmidt G. (1998) Constraints on Earth accretion deduced from noble metals in the oceanic mantle. *Nature* **391**, 166–169.

Stone W. E., Crocket J. H., Fleet M. E. and Larson M. S. (1996) PGE mineralization in Archean volcanic systems: Geochemical evidence from thick, differentiated mafic-ultramafic flows, Abitibi greenstone belt, Ontario, and implications for exploration. *Journal of Geochemical Exploration* **56**, 237–263.

Swartzendruber and Sundman (1983) The Fe-Ru (Iron-Ruthenium) system. *Bulletin of Alloy Phase Diagrams* **4**, 155–160.

Sylvester P. J. and Eggins S. M. (1997) Analysis of Re, Au, Pd, Pt and Rh in NIST glass certified reference materials and natural basalt glasses by Laser Ablation ICP-MS. *Geostandards Newsletter* **21**, 215–229.

Thompson J. B. (1967) Thermodynamic properties of simple solutions. In: *Researches in geochemistry* (ed. P. H. Abelson). Wiley, New York, pp. 340–361.

Tomiska J. (1989) Massenspektroskopische Ermittlung der thermodynamischen Mischungsgrößen in der kfz-Phase und Berechnung des Schmelzdiagramms Eisen-Palladium. *Zeitschrift für Metallkunde* **80**, 888–893.

Toulmin III P. and Barton Jr P. B. (1964) A thermodynamic study of pyrite and pyrrhotite. *Geochimica et Cosmochimica Acta* **28**, 641–671.

Tredoux M., Lindsay N. M., Davies G., McDonald L. (1995) The fractionation of platinum-group elements in magmatic systems with the suggestion of a novel causal mechanism. *South African Journal of Geology* **98**, 157–167.

Tuff J. and O'Neill H. S. (2010) The effect of sulfur on the partitioning of Ni and other first-row transition elements between olivine and silicate melt. *Geochimica et Cosmochimica Acta* **74**, 6180–6205.

Van Achterbergh E., Ryan C. G., Jackson S. E. and Griffin W. L. (2001) Data reduction software for LA-ICP-MS. In: *Laser Ablation-ICPMS in the Earth Sciences, Principles and Applications*, MACShort Course, vol. 29 (ed. P. Sylvester), pp. 239–243.

Wallace P. and Carmichael I. S. E. (1992) Sulfur in basaltic magmas. *Geochimica et Cosmochimica Acta* **56**, 1863–1874.

Walter M. J., Newsom H. E., Ertel W. and Holzheid A. (2000) Siderophile elements in the Earth and Moon: Metal/silicate partitioning and implications for core formation. In: *Origin of the Earth and Moon* (eds. R. Canup and K. Righter). University of Arizona Press.

Wänke H. (1981) Constitution of the terrestrial planes. *Philosophical Transactions of the Royal Society London A* **303**, 287–302.

Wohlgemuth-Ueberwasser C. C., Ballhaus C., Berndt J., Paliulionyte V. S. N. and Meisel T. (2007) Synthesis of PGE sulfide standards for laser ablation inductively coupled plasma mass spectrometry (LA-ICP-MS). *Contributions to Mineralogy and Petrology* **154**, 607–617.

Woodhead S. J., Pearson D. G. and Thirlwall M. F. (2002) A platinum group element and Re–Os isotope investigation of siderophile element recycling in subduction zones: comparison of Grenada, Lesser Antilles arc, and the Izu-Bonin arc. *Journal of Petrology* **43**, 171–198.

Yokoyama T., Walker D. and Walker R. J. (2009) Low osmium solubility in silicate at high pressures and temperatures. *Earth and Planetray Science Letters* **279**, 165–173.

Danksagung

An dieser Stelle möchte ich mich bei den vielen Menschen bedanken, die auf die eine oder die andere Art dazu beigetragen haben, dass “das Buch” nun endlich existiert.

Zuallererst möchte ich mich bei Chris Ballhaus bedanken, der es mir ermöglicht hat, diese Arbeit anzufertigen. Chris hat mit vielen Ideen und Diskussionen wesentlich zum Gelingen dieser Arbeit beigetragen. Gleiches gilt auch für Raúl Fonseca, der mir immer mit Rat und Tat zur Seite gestanden hat. Thorsten Geisler-Wierwille danke ich herzlich dafür, dass er wieder eine Arbeit von mir begutachtet.

Besonderer Dank gilt Klaus Peter Jochum, Brigitte Stoll und Ulrike Weis vom MPI in Mainz für die LA-ICP-MS Analysen und für das Aufbewahren meiner Laborbücher. Paul Sylvester und Mike Tubrett sei ebenfalls für LA-ICP-MS Analysen gedankt. Außerdem möchte ich Harald Euler und Bruno Barbier für die XRD-Analysen danken.

Besonders bedanken möchte ich mich auch bei Henrik Blanchard, Andreas Vogt, und dem gesamten Team der Werkstätten in Bonn und Köln, für die stete Bereitschaft meine großen und kleinen Problemchen zu lösen. Ohne ihre Hilfe wäre das 1-atm Labor wohl niemals ans Laufen gekommen. Carsten Münker sei an dieser Stelle gedankt für den Zugang zum 1-atm Labor in Köln. Weiterhin sei allen guten Schlossgeistern gedankt für die vielen, manchmal zu alltäglichen, großen und kleinen Dinge.

Ein großes Danke an alle Schlossbewohner für die netten Runden im Kaffeeraum oder beim Grillen: Maria (du hast das Rennen gewonnen!), Raúl, Elis, Dani, Daniel, Simone, Anne, Thorsten, Stephan P., Schuthi, Stella, Toni, Claudia, Cora, Stephan K., Ambre, Jude, Jo, Ashlea, Alessandro, Silke, Jacek, Frank, und alle die ich vergessen haben sollte.

Nicht zuletzt bedanke ich mich bei meiner Familie, dass sie mich immer angespornt, und Dachlatten geschickt haben. Alex, gut, dass es dich gibt!

Et hätt noch emmer joot jejange!

Publikationen

Artikel in begutachteten Zeitschriften

- Fonseca R.O.C., Mallmann G., O'Neill H.St.C., Campbell I. H. and Laurenz V. (2011) Solubility of Os and Ir in sulfide melt: Implications for Re/Os fractionation during partial melting. *Earth and Planetary Science Letters* **311**, 339–350.

- Helmy H.M., Ballhaus C., Wohlgemuth-Ueberwasser C., Fonseca R.O.C., Laurenz V. (2010) Partitioning of Se, As, Sb, Te and Bi between monosulfide solid solution and sulfide melt – application to magmatic sulfide deposits. *Geochimica et Cosmochimica Acta* **74**, 6174–6179.

- Laurenz V., Fonseca R.O.C., Ballhaus C., Sylvester P.J. (2010) Solubility of Palladium in picritic melts: 1. The effect of FeO. *Geochimica et Cosmochimica Acta* **74**, 2989–2998.

- Ballhaus C., Bockrath C., Wohlgemuth-Ueberwasser C., Laurenz V., Berndt J. (2006) Fractionation of the noble metals by physical processes. *Contributions to Mineralogy and Petrology* **152**, 667–684.

Konferenzbeiträge

- Laurenz V., Fonseca R.O.C., Ballhaus C., Jochum K.P., Sylvester P.J. (2011) The effect of fS_2 on PGE solubility in silicate melts. Goldschmidt Conference Abstracts, *Mineralogical Magazine* **75**, A 1275.

- Ballhaus C., Laurenz V., Fonseca R., Münker C., Albarede F., Rohrbach A., Schmidt M.W., Jochum K.P., Stoll B., Weis U., Helmy H. (2011) Late volatile addition to Earth. Goldschmidt Conference Abstracts, *Mineralogical Magazine* **75**, A 475.

- Laurenz V., Ballhaus C., Fonseca R.O.C., Jochum K.P., Sylvester P.J. (2010) The effect of fS_2 on PGE solubility in silicate melts - Implications for ore forming processes. *European Journal of Mineralogy* **20**, electronic supplement, So6-T04.

- Laurenz V., Ballhaus C., O'Neill, H.St.C., Wohlgemut-Ueberwasser C.C., Fonseca R.O.C. (2009) Ir partitioning between chromite and silicate melt – The influence of fO_2. *Geochimica et Cosmochimica Acta* **73**, Supplement S, A 727.

- Fonseca R.O.C., Laurenz V., Ballhaus C., Sylvester P. J. (2009) How extensive is the effect of Fe and S on the solubility of PGE in silicate melts? *Geochimica et Cosmochimica Acta* **73**, Supplement S, A389 .

- Ballhaus C., Laurenz V., Fonseca R.O.C., Sylvester P. J. (2009) PGE enrichment in sulfide melt – role of the R factor. 10th Biennial Meeting of the SGA, extended abstract, A047.

- Laurenz V., Fonseca R.O.C., Ballhaus C. (2008) Enrichment of PGE in sulfides: New insights from Pd solubility in silicate melts. *European Journal of Mineralogy* **19**, electronic supplement, Abstract No. 518.

- Laurenz V., Ballhaus C., Fonseca R.O.C. (2008) Effect of fS_2 on Pd solubility in silicate melts – Implications for PGE enrichment processes in sulfide melts. *Geochimica et Cosmochimica Acta* **72**, A519.

- Ballhaus C., Laurenz V., Fonseca R.O.C. (2008) Enrichment of the PGE in magmatic sulfide melt. *Geochimica et Cosmochimica Acta* **71**, Supplement 1, A 49.

- Laurenz V., Wohlgemuth-Ueberwasser C., Ballhaus C. (2007) Experimental determination of Iridium solubility in silicate melts. *Geochimica et Cosmochimica Acta* **71**, Supplement 1, A547.

- Laurenz V., Wohlgemuth-Ueberwasser C., Berndt J., Ballhaus C. (2006) Behaviour of Ir in chromite-saturated silicate melt - Experiments and LA-ICP-MS analysis. *Geochimica et Cosmochimica Acta* **70**, Supplement 1, A344.

- Laurenz V., Bockrath C., Holzheid A., Ballhaus C. (2004): Iridium Einbau in Chromspinell? *European Journal of Mineralogy* **16**, Beihefte: 58.

Bonn, Februar 2012